



HAL
open science

Ad hoc angular discretization of the radiative transfer equation

Y. Favennec, T. Mathew, Mohd Afeef Badri, Pierre Jolivet, Benoit Rousseau,
D. Lemonnier, P.J. Coelho

► **To cite this version:**

Y. Favennec, T. Mathew, Mohd Afeef Badri, Pierre Jolivet, Benoit Rousseau, et al.. Ad hoc angular discretization of the radiative transfer equation. *Journal of Quantitative Spectroscopy and Radiative Transfer*, 2019, 225, pp.301-318. 10.1016/j.jqsrt.2018.12.032 . hal-02333870

HAL Id: hal-02333870

<https://hal.science/hal-02333870>

Submitted on 14 Jan 2021

HAL is a multi-disciplinary open access archive for the deposit and dissemination of scientific research documents, whether they are published or not. The documents may come from teaching and research institutions in France or abroad, or from public or private research centers.

L'archive ouverte pluridisciplinaire **HAL**, est destinée au dépôt et à la diffusion de documents scientifiques de niveau recherche, publiés ou non, émanant des établissements d'enseignement et de recherche français ou étrangers, des laboratoires publics ou privés.

Ad hoc angular discretization of the RTE

Y. Favennec^{a,*}, T. Mathew^a, M. A. Badri^{a,b}, P. Jolivet^c, B. Rousseau^a, D. Lemonnier^d,
P.J. Coelho^e

^a*Laboratoire de Thermique et Énergie de Nantes, UMR CNRS 6607, Polytech' Nantes, Université de Nantes, 44306 Nantes, France*

^b*Institut de Recherche Technologique Jules Verne, 44340 Bouguenais, France*

^c*CNRS, Institut de Recherche en Informatique de Toulouse, 31062 Toulouse, France*

^d*Institut P', CNRS, ISAE ENSMA, 86961 Futuroscope Chasseneuil cedex, France*

^e*Mechanical Engineering Department, Instituto Superior Técnico, Technical University of Lisbon, Av. Rovisco Pais, 1049-001 Lisboa, Portugal*

Abstract

Solving the radiative transfer equation with the finite element method requires both angular and spatial discretizations. We develop a novel algorithm of angular mesh discretization based on a posteriori calculations. The obtained angular discretizations are optimized in such a way that they suit the particular physics under consideration. Such ad hoc angular discretizations are implemented for increasing the finite element solution efficiency. Using comparative numerical tests based on the solution accuracy, the solutions provided by the obtained ad hoc discretizations are proven to be better than the ones provided by the standard uniform angular discretizations. The algorithm is drafted in such a way that it could be easily implemented using pre-existing open-source mathematical libraries. This paper is an extended version of a paper presented at the CTRPM-VI conference [1]. As an extension to the two-dimensional version presented at the conference, a three-dimensional adaptive ad hoc angular discretization of the RTE is addressed here.

1. Introduction

A radiative transfer phenomena is often characterized by the knowledge of its radiative intensity field I . For steady-state monochromatic radiative transfer problems, the radiation intensity turns out to be a function of five variables, $I = I(x, y, z, \theta, \phi)$: three spatial position variables $\mathbf{x} = (x, y, z)$ and two angular variables (θ, ϕ) defining the propagation direction $\mathbf{s} = \mathbf{s}(\theta, \phi)$. In order to acquire the radiative intensity field for a particular problem of interest, most practitioners numerically solve the radiative transfer equation (RTE). One of the methods to numerically solve the RTE is the finite element method (FEM). The numerical solution of the RTE with the FEM needs discretizations in both spatial and angular domains, hence concurrently requiring spatial and angular meshes. In the context of finite elements, the spatial discretization allows one to build an approximate functional space in

*Corresponding author.

which the space-dependent contribution of the radiative intensity is searched for. In the same way, the angular discretization with the FEM allows one to build an approximate functional space in which the angular-dependent contributions of the radiative intensity are searched for.

During the past decades the FEM has grown in popularity and at present it is considered among the most popular and versatile numerical methods for solving diverse scientific problems, including solid mechanics, fluid mechanics, electromagnetics, heat transfer, etc. Due to its strong mathematical developments, the FEM allows theoretical studies such as uniqueness, consistency, existence and stability of solution to be performed. Moreover the method is well suited for unstructured grids which eases the solution process for complex geometries. Fortunately, an additional advantage of the FEM is its consistent discretization, allowing us to apply the a posteriori error control techniques which gives rise to mesh adaptation. Via this article we intend to exploit this particular advantage of the FEM, the a posteriori error control, and use it to build ad hoc angular meshes which would consequently reduce computational loads while maintaining the accuracy of the solution.

While the FEM, the finite volume method (FVM), the finite difference method, etc., may be used for spatial discretization of the RTE, for its angular discretization it is common within the radiative transfer community to use the discrete ordinates method (DOM), or the FVM. Alternatively, as is done in this paper, researches also use the FEM for discretizing the angular space. Hence, to fully discretize the RTE, the following few discretization methods are being used: DOM-FVM [2], DOM-FEM [3], FVM-FVM [4], FEM-FEM [5], FEM-FVM [6], etc., (first acronym abbreviates the angular discretization, the second one abbreviates the spatial discretization). Within this article we will employ the FEM-FEM discretization on the RTE.

In this paper, we approximate the angular functional space using vertex-based piece-wise constant functions, while continuous piece-wise linear functions are chosen for the spatial functional space. The \mathbb{P}_0 FEM for the angular space results in a similar approach as the DOM, i.e., one obtains a system of semi-discrete radiative transfer equations which further need the spatial discretization treatment, see [5]. Due to similarities between the \mathbb{P}_0 angular FEM discretization and the DOM, a symmetric angular mesh obtained from the S_n or the T_n quadrature, [2], or based on a polyhedron refinement [7], etc., is usually used. Usually such discretizations yield a distribution of directions very uniform in the space of the unit sphere. If the moment conditions are satisfied, it is well accepted that accurate solutions can be found for many radiative transfer problems.

However, in many radiative transfer scenarios e.g.: i) when the considered geometry of participating medium is highly complex; ii) when strong specular reflections occur on boundaries of the medium; and iii) when considering a physical phenomenon involving dominant directions for the radiative intensity propagation; in all these cases one either needs a very fine angular mesh that demands huge computational resources, or an alternate smart way which considers ad hoc angular discretizations.

Consider the example of the numerical simulations performed with the DOM-FEM in [8]. Within the article the primary test case is of a collimated laser beam was impinging a strut of

an open-cell foam. The impinging direction was quasi-orthogonal to the longitudinal axis of the strut. It has been shown that this strut could not be represented by a cylinder, because the spatial topology was irregular. So, due to the presence of specular reflections, some dominant directions of propagation of the radiative intensity could be observed. In order to model the involved physics accurately, it was proven that a unit sphere discretization with at least 320 directions was necessary. As such, high computational resources and time were required to solve such problem without considering the setting of vectorial finite elements [9] and associate parallelization tools [10]. A similar scenario was noticed in [11, 12], who used the FEM-FEM discretization and ended up using 1280 directions with an adaptive mesh for astrophysics problems.

The intent of this study is thus to reduce the high number of degrees of freedom for the sphere discretization, while reaching better accuracy of the solution. In other terms, the goal is to reduce the size of the linear system to be solved, yielding less computational time and resources, without altering the solution. We do so by developing an angular adaptivity algorithm based on an a posteriori error estimation using vertex-based \mathbb{P}_0 Lagrange functions built on the triangulation of the unit sphere. In order to highlight to what extent the present methodology differs from the literature, let us give some major elements of bibliography on the subject of angular finite elements and angular adaptivity dedicated to the solution of the RTE.

In 2001, [7] used finite elements for the angular discretization of the RTE, for astrophysics applications. The angular mesh was based on the uniform icosahedron at the first and second levels of refinement, involving 80 and 320 ordinates, respectively. In order to discretize the angular space, the zeroth-order FE space was used (piecewise constant trial functions). As stated in this article, the benefit relies essentially in the equally distributed quadrature points. Also, they claim that their scheme is second order accurate in the evaluated ordinate points, due to the super-convergence property.

In 2005, [6] developed a hybrid finite volume/finite element discretization of the radiative transfer equation with application to multi-dimensional heat transfer in rectangular enclosures with gray absorbing, emitting and scattering media. The angular discretization was performed by means of lines of constant latitude and longitude. The first order FE space was used for the angular discretization.

In 2008, [13] used discontinuous functions on spherical triangles based on uniformly refined icosahedra, the RTE being simplified to non-scattering physics. Also, wavelet bases was used for mesh adaptivity. Doing so, they could reduce the number of the degrees of freedom by a factor of ten while still retaining the accuracy of the scheme. Elsewhere, [14] showed that the local angular adaptivity was an efficient tool for a variety of two-dimensional particle transport calculations, when coupled with interpolative methods such as the simple linear, and the linear in sine and cosine.

In 2009, [15] developed a fast solver coupling discrete ordinates based on a uniform discretization and finite elements for the space, the iterative solver being extended from the source iteration to a block-based Gauss-Seidel approach.

In 2010, in [16], the RTE has been coupled with its diffusion approximation counterpart,

for optical tomography applications through fluorescence imaging. As above, the angular discretization was performed by means of lines of constant latitude and longitude. As an extension of the work proposed by [17], starting out from the second-order even-parity of the RTE, [18] derived a finite element discretization of the spatial and angular domains on the second-order even-parity equation. The main goal was to avoid the well-known ray-effect. In this article, the discretization was also performed based on the octahedron.

In 2011, [19] performed a comparison of different angular discretization schemes for the solution of the RTE in non-scattering media. More specifically, they performed angular discretization by means of quadrangles (lines of constant latitude and longitude) on the one hand, and triangles on the other hand (based on the Thurgood discretization [20]). Integrations were then performed through a finite volume method. According to this study, triangles perform better than quadrangles, especially for optical thin media and optically intermediate media. Another conclusion was that, when ray effect is present, finite volume based on triangular discretization is more accurate than ordinary DOM.

In 2015, [5] developed a full finite element model for both space and angles for the modeling of multi-dimensional radiative transfer in participating media, including scattering. The angular discretization was performed with angular finite elements (AFEM) based on the Galerkin approach. As they claim, such an implementation is ideally suited for h and/or p refinement(s). Zero and first order Lagrange functions have been developed on (quasi)-uniform triangular elements based on the octahedron, and tested successfully on different cases. Elsewhere, [21] implemented a goal-based angular adaptivity with wavelet-based discretizations. It is shown there, on several examples, how adaptivity could reduce drastically the number of degrees of freedom while not altering the solution at all. Such a strategy, initially developed for neutronic applications, has been extended later on to thermal radiation modeling in non grey media [22]. [23] also proposed a local angular refinement for the RTE coupled with space and angular discontinuous Galerkin finite element approach. In this study, they particularly emphasized on the derivation of the upwinding scheme needed due to the use of the discontinuous discretization.

In 2016, [24] presented a mapping algorithm required for passing, within a discontinuous angular finite element approach, the angular flux solution between spatial regions with different angular quadrature refinement. According to them, this algorithm is efficient for mapping sufficiently smooth solutions away from octant boundaries. The angular quadrature is based on the successive refinement of the three spherical quadrilaterals defining an octant.

In 2017, [3] developed a particular treatment of the specular reflection for the 3D radiative transfer equation solved with the discrete ordinates method based on the sphere discretization. Discretizations based on the refinement of both the Thurgood method and the Lee method [25] have both been used. The new so-called S_qT_{pn} discretization scheme have been also introduced. One of the main contribution of this paper was the implementation of the specular reflection for complex spatial geometries. As an extension of this work, [8] applied such developments on a highly complex geometry given by a x-ray tomography data of a silicon-carbide ligament of an open-cell foam. It was shown that a large number of angular directions had to be used in order to get an accurate solution.

The proposed methodology differs from studies conducted in the past for, at least, three reasons. First, the ad hoc angular discretization is obtained from an arbitrary sphere triangulation without any other predefined rule. This allows one to use any finite element mesh generator such as [26], for constructing the mesh of the unit sphere. However, it should be mentioned that meshes based on the octahedron, the icosahedron, the S_n quadrature, or the T_n quadrature can also be plugged in for obtaining the ad hoc angular discretization. Second, the examples of angular adaptation dealt with in this paper involve the specular reflection. It is well known that such a physics is highly difficult to handle. In the very best of our knowledge, the coupling of specular reflection with angular adaptivity has never been studied before. Lastly, after proving on two academic cases that angular adaptivity can give more accurate results with much less directions than with fine uniform discretizations, the proposed methodology has been tested on a complicated three-dimensional geometry. This one contains a smooth curved boundary allowing a very high number of directions to be taken into account if accuracy is the purpose. Such a modeling mimics a real-life material forming process.

The remainder of the paper is organized as follows. Section 2 gives the main ingredients for the angular finite element setting. It particularly emphasizes on the computation of matrices arising from the angular discretization, on the specular reflection treatment within a finite element context, the definition of balls and spheres, and the mappings between these mathematical objects. Section 3 describes how the ad hoc angular discretization is found from the radiative transfer solver outputs, and the use of an external library for the adaptation process itself. Particularly, the vertex-based \mathbb{P}_0 finite element space is introduced. Section 4 then presents briefly the vectorial finite element setting for the spatial discretization. Section 5 is then dedicated to numerical applications where it is particularly shown how ad hoc discretizations can give results unattainable with other standard uniform discretizations. The paper ends with some conclusions and remarks.

2. Angular discretization of the RTE with the FEM

Within this section the FE angular discretization phase for the RTE is explained in details. We start by introducing the RTE in its integro-differential form (1), and by following the variational principles of finite element methods to finally deduce a system of coupled partial differential equations (29).

2.1. Derivation of the formulation

Let the problem of solving the RTE be: search $I(\mathbf{x}, \mathbf{s}) : \mathcal{D} \times \mathcal{S}^2 \mapsto \mathbb{R}$ that satisfies:

$$\mathbf{s} \cdot \nabla I(\mathbf{x}, \mathbf{s}) + (\kappa + \sigma_s)I(\mathbf{x}, \mathbf{s}) - \sigma_s \int_{\mathcal{S}^2} I(\mathbf{x}, \mathbf{s}')\phi(\mathbf{s}, \mathbf{s}') \, d\mathbf{s}' - \kappa I_b(\mathbf{x}) = 0. \quad (1)$$

Here, κ , σ_s , ϕ , and I_b are positive functions (inputs to the RTE) and represent the absorption coefficient, the scattering coefficient, the scattering phase function, and the Plankian black body intensity of the medium of interest, respectively. One could refer to [27] for detailed explanations of the RTE.

In an angular finite element context, a functional space is defined by:

$$V^s = \{v(\mathbf{s}) \in L_2(\mathcal{S}^2)\}, \quad (2)$$

which means that V^s is the set of square integrable functions on the unit sphere. The unit sphere \mathcal{S}^2 is triangulated such that its approximation, say \mathcal{S}_h^2 , is the union of elements \mathcal{T}_j^s , $j \in \llbracket 1; N_d \rrbracket$. On such a discretized unit sphere, an approximated functional space $V_h^s \subset V^s$ is henceforth to be used for setting up the variational formulation. The RTE is multiplied by a test function, say $\Psi(\mathbf{s}) \in V_h^s$, and the resulting product is integrated over the whole angular computational domain \mathcal{S}_h^2 . Note that the subscript h is avoided from here on, so \mathcal{S}^2 (resp. V^s) should be read as \mathcal{S}_h^2 (resp. V_h^s). The radiative problem consists in searching $I(\mathbf{x}, \mathbf{s}) \in V^s$ such that

$$\int_{\mathcal{S}^2} \left[\mathbf{s} \cdot \nabla I(\mathbf{x}, \mathbf{s}) + (\kappa + \sigma_s)I(\mathbf{x}, \mathbf{s}) - \sigma_s \int_{\mathcal{S}^2} I(\mathbf{x}, \mathbf{s}')\phi(\mathbf{s}, \mathbf{s}') \, d\mathbf{s}' - \kappa I_b(\mathbf{x}) \right] \Psi(\mathbf{s}) \, d\mathbf{s} = 0, \quad \forall \Psi(\mathbf{s}) \in V^s. \quad (3)$$

Further, let $\{\varphi_i(\mathbf{s})\}_{i=1}^{N_d}$ be a basis of V^s such that a function $u(\mathbf{s}) \in V^s$ can be expressed, with no loss of generality, as the discrete summation:

$$u(\mathbf{s}) = \sum_{i=1}^{N_d} \varphi_i(\mathbf{s})u(\mathbf{s}_i). \quad (4)$$

Rather than expressing the weak formulation for all $\Psi(\mathbf{s})$, the weak formulation is expressed for all test functions $\varphi_j(\mathbf{s})$. Let us derive each term separately.

- Transport:

$$\begin{aligned} \int_{\mathcal{S}^2} \mathbf{s} \cdot \nabla I(\mathbf{x}, \mathbf{s}) \varphi_j(\mathbf{s}) \, d\mathbf{s} &= \int_{\mathcal{S}^2} \mathbf{s} \cdot \sum_i \nabla I(\mathbf{x}, \mathbf{s}_i) \varphi_i(\mathbf{s}) \varphi_j(\mathbf{s}) \, d\mathbf{s} \\ &= \sum_i \int_{\mathcal{S}^2} \varphi_i(\mathbf{s}) \varphi_j(\mathbf{s}) \mathbf{s} \, d\mathbf{s} \cdot \nabla I(\mathbf{x}, \mathbf{s}_i) \\ &= \sum_i \mathbf{a}(\varphi_i, \varphi_j) \cdot \nabla I(\mathbf{x}, \mathbf{s}_i) \\ &= \sum_{\alpha=\{x,y,z\}} \sum_i a^\alpha(\varphi_i, \varphi_j) \partial_\alpha I(\mathbf{x}, \mathbf{s}_i); \end{aligned} \quad (5)$$

- extinction:

$$\begin{aligned} \int_{\mathcal{S}^2} (\kappa + \sigma_s)I(\mathbf{x}, \mathbf{s}) \varphi_j(\mathbf{s}) \, d\mathbf{s} &= (\kappa + \sigma_s) \int_{\mathcal{S}^2} \sum_i I(\mathbf{x}, \mathbf{s}_i) \varphi_i(\mathbf{s}) \varphi_j(\mathbf{s}) \, d\mathbf{s} \\ &= (\kappa + \sigma_s) \sum_i \int_{\mathcal{S}^2} \varphi_i(\mathbf{s}) \varphi_j(\mathbf{s}) \, d\mathbf{s} I(\mathbf{x}, \mathbf{s}_i) \\ &= (\kappa + \sigma_s) \sum_i b(\varphi_i, \varphi_j) I(\mathbf{x}, \mathbf{s}_i); \end{aligned} \quad (6)$$

- scattering:

$$\begin{aligned}
\int_{\mathcal{S}^2} \sigma_s \int_{\mathcal{S}^2} I(\mathbf{x}, \mathbf{s}') \phi(\mathbf{s}, \mathbf{s}') \, d\mathbf{s}' \, \varphi_j(\mathbf{s}) \, d\mathbf{s} &= \int_{\mathcal{S}^2} \sigma_s \int_{\mathcal{S}^2} \sum_i I(\mathbf{x}, \mathbf{s}_i) \phi(\mathbf{s}, \mathbf{s}_i) \varphi_i(\mathbf{s}') \, d\mathbf{s}' \, \varphi_j(\mathbf{s}) \, d\mathbf{s} \\
&= \sigma_s \int_{\mathcal{S}^2} \sum_i I(\mathbf{x}, \mathbf{s}_i) \phi(\mathbf{s}, \mathbf{s}_i) \int_{\mathcal{S}^2} \varphi_i(\mathbf{s}') \, d\mathbf{s}' \, \varphi_j(\mathbf{s}) \, d\mathbf{s} \\
&= \sigma_s \sum_i I(\mathbf{x}, \mathbf{s}_i) \int_{\mathcal{S}^2} \varphi_i(\mathbf{s}) \, d\mathbf{s} \int_{\mathcal{S}^2} \phi(\mathbf{s}, \mathbf{s}_i) \varphi_j(\mathbf{s}) \, d\mathbf{s} \\
&= \sigma_s \sum_i c(\varphi_i, \varphi_j) I(\mathbf{x}, \mathbf{s}_i);
\end{aligned} \tag{7}$$

- source by emission:

$$\begin{aligned}
\int_{\mathcal{S}^2} \kappa I_b(\mathbf{s}) \, \varphi_j(\mathbf{s}) \, d\mathbf{s} &= \kappa I_b \int_{\mathcal{S}^2} \varphi_j(\mathbf{s}) \, d\mathbf{s} \\
&= \kappa I_b \ell(\varphi_j).
\end{aligned} \tag{8}$$

Taking into account all terms, we yield angular discretized RTE, which reads: search $I(\mathbf{x}, \mathbf{s}_i)$, $i \in \llbracket 1; N_d \rrbracket$ such that, $\forall j \in \llbracket 1; N_d \rrbracket$:

$$\sum_{\alpha=\{x,y,z\}} \sum_i a^\alpha(\varphi_i, \varphi_j) \partial_\alpha I(\mathbf{x}, \mathbf{s}_i) + (\kappa + \sigma_s) \sum_i b(\varphi_i, \varphi_j) I(\mathbf{x}, \mathbf{s}_i) = \sigma_s \sum_i c(\varphi_i, \varphi_j) I(\mathbf{x}, \mathbf{s}_i) + \kappa I_b \ell(\varphi_j). \tag{9}$$

We thus have N_d linear equations with N_d unknowns. At this stage, the semi-discretized unknowns are still continuous in space. The N_d linear relationships written above can be set up with corresponding matrices. To do so, a matrix \mathcal{A}^α is defined for each transport operator $\mathbf{s}_\alpha \cdot \partial_\alpha I$, $\alpha = x, y, z$, a matrix \mathcal{B} is defined for the extinction operator, a matrix \mathcal{C} is defined for the scattering operator, and a vector \mathcal{L} is used to express the emission:

$$\begin{aligned}
\mathcal{A}_{i,j}^\alpha &= a^\alpha(\varphi_i, \varphi_j) = \int_{\mathcal{S}^2} \varphi_i(\mathbf{s}) \, \varphi_j(\mathbf{s}) \, \mathbf{s}_\alpha \, d\mathbf{s}; \\
\mathcal{B}_{i,j} &= (\kappa + \sigma) b(\varphi_i, \varphi_j) = (\kappa + \sigma_s) \int_{\mathcal{S}^2} \varphi_i(\mathbf{s}) \, \varphi_j(\mathbf{s}) \, d\mathbf{s}; \\
\mathcal{C}_{i,j} &= \sigma_s c(\varphi_i, \varphi_j) = \sigma_s \int_{\mathcal{S}^2} \varphi_i(\mathbf{s}) \, d\mathbf{s} \int_{\mathcal{S}^2} \phi(\mathbf{s}, \mathbf{s}_i) \varphi_j(\mathbf{s}) \, d\mathbf{s}; \\
\mathcal{L}_j &= \kappa I_b \ell(\varphi_j) = \kappa I_b \int_{\mathcal{S}^2} \varphi_j(\mathbf{s}) \, d\mathbf{s}.
\end{aligned} \tag{10}$$

The semi-discretized problem consists, at this stage, in searching $\mathbf{I}(\mathbf{x}) = \{I_j\}_{j=1}^{N_d}(\mathbf{x})$ that satisfies:

$$\sum_{\alpha=\{x,y,z\}} [\mathcal{A}^\alpha \partial_\alpha \mathbf{I}] + \mathcal{B} \mathbf{I} - \mathcal{C} \mathbf{I} - \mathcal{L} = 0. \tag{11}$$

Remark 1 (Alternate formulation). Let us denote $\text{diag}(\mathcal{A})$ the diagonal of the matrix \mathcal{A} and $\overline{\mathcal{A}}$ the out-of diagonal part. (One has $\mathcal{A} = \text{diag}(\mathcal{A}) + \overline{\mathcal{A}}$.) The matrix form (11) can be re-written as:

$$\sum_{\alpha=\{x,y,z\}} [\text{diag}(\mathcal{A}^\alpha)\partial_\alpha\mathbf{I}] + \text{diag}(\mathcal{B})\mathbf{I} + \sum_{\alpha=\{x,y,z\}} [\overline{\mathcal{A}^\alpha}\partial_\alpha\mathbf{I}] + (\overline{\mathcal{B}} - \mathcal{C})\mathbf{I} - \mathcal{L} = 0. \quad (12)$$

This formulation can be useful later on, when choosing the \mathbb{P}_0 finite element basis.

Remark 2 (Normalization). Because the normalization is to be done on the scattering operator matrix, the construction of this matrix is performed following these steps, for all $i \in \llbracket 1; N_d \rrbracket$:

1. compute $\mathcal{C}_{i,j} = \int_{\mathcal{S}^2} \phi(\mathbf{s}, \mathbf{s}_i) \varphi_j(\mathbf{s}) \, d\mathbf{s}$ and the sum: $\zeta_i = \sum_j \mathcal{C}_{i,j}$, $\forall j \in \llbracket 1; N_d \rrbracket$;
2. normalize $\mathcal{C}_{i,j} \leftarrow \mathcal{C}_{i,j}/\zeta_i$, $\forall j \in \llbracket 1; N_d \rrbracket$;
3. compute $\mathcal{C}_{i,j} \leftarrow \sigma_s \int_{\mathcal{S}^2} \varphi_i(\mathbf{s}) \, d\mathbf{s} \times \mathcal{C}_{i,j}$, $\forall j \in \llbracket 1; N_d \rrbracket$.

2.2. Specular reflection

The treatment of the specular reflection consists in considering that an incident intensity on the spatial boundary $\partial\mathcal{D}$, characterized locally by its outward unit normal vector \mathbf{n} , that travels along the direction \mathbf{s} such that $\mathbf{s} \cdot \mathbf{n} > 0$, is reflected towards the direction $\mathbf{R}(\mathbf{n})\mathbf{s}$. This intensity is attenuated due to the process of reflection. The ratio between the reflected intensity and the incident intensity is the specular reflectivity coefficient ρ . This reflectivity coefficient is an explicit function of the angle between the reflected beam and the outward normal vector characterizing locally the boundary surface. One may write, $\forall \mathbf{x} \in \partial\mathcal{D}$:

$$I^\vee(\mathbf{x}, \mathbf{R}\mathbf{s}) = \rho_s(\mathbf{s} \cdot \mathbf{n})I(\mathbf{x}, \mathbf{s}), \quad (13)$$

or equivalently, with $\zeta(\mathbf{s}) = \mathbf{R}^{-1}(\mathbf{n})\mathbf{s}$, and using the same notations as in [3]:

$$I^\vee(\mathbf{x}, \mathbf{s}) = \rho_s(\mathbf{s} \cdot \mathbf{n})I(\mathbf{x}, \zeta(\mathbf{s})). \quad (14)$$

This relationship is continuous in angles. Hence, considering finite element approximation in angles on the RTE itself demands approximating also this continuous boundary condition relationship. In discrete form, (14) is rewritten to:

$$I_m^\vee(\mathbf{x}) = \rho_s(\mathbf{s}_m \cdot \mathbf{n}) \sum_{\mathbf{s}_j \cdot \mathbf{n} > 0} \delta_{m,j}(\mathbf{n}) I_j(\mathbf{x}) \quad \forall m \in \llbracket 1; N_d \rrbracket, \mathbf{s}_m \cdot \mathbf{n} < 0. \quad (15)$$

In this relationship, $\delta_{m,j}(\mathbf{n})$, $(m, j) \in \llbracket 1; N_d \rrbracket^2$ are partition ratio coefficients. The partition ratio coefficient $\delta_{m,j}$ represents the part of the energy associated to the degree of freedom j which is given to the degree of freedom m . In order to respect equilibrium in terms of incident and reflected energies, the relationship (15) must respect the following partition rule:

$$\sum_{\mathbf{s}_m \cdot \mathbf{n} < 0} \delta_{m,j}(\mathbf{n}) = 1 \quad \forall j \in \llbracket 1; N_d \rrbracket, \mathbf{s}_j \cdot \mathbf{n} > 0. \quad (16)$$

In a previous work, [3], the partition ratio coefficients were calculated following these three steps: i) the considered solid angle was reflected on the boundary, either fully or partially; ii) this reflected solid angle being very unlikely corresponding to any existing solid angle, the area of intersection of it with all others was calculated; iii) the partition ratio coefficient was calculated thanks to the ratio between surfaces. All calculations were performed analytically using geometric transformations as a pre-process operation. This strategy was highly accurate and totally coherent with the discrete ordinates method based on the sphere discretization.

In the strategy proposed in this paper, the reflection operation is performed in a finite element context. Let a trial function $u(\mathbf{s}) \in V^s$, and further let us write formally $v(\mathbf{s}) = u(\mathbf{R}\mathbf{s})$, with $\mathbf{R}(\mathbf{n}) = 2\mathbf{n}\mathbf{n}^\top - I$ the Householder rotation matrix [28], and project this function onto the finite element space V^s . Partition ratio coefficients are then calculated spanning the whole basis $\{\varphi_k(\mathbf{s})\}_{k=1}^{N_d}$ of V^s for u , and calculate the energy ratio:

$$\delta_{k,l}(\mathbf{n}) = \frac{\int_{S^2} \varphi_l(\mathbf{R}\mathbf{s})\varphi_k(\mathbf{s}) \, d\mathbf{s}}{\int_{S^2} \varphi_l(\mathbf{s}) \, d\mathbf{s}}. \quad (17)$$

This strategy is simple to implement, and both orders zero and one can be implemented in a straightforward manner. Moreover, the equality constraint (16) is not to be explicitly prescribed.

With the order zero angular finite element discretization, this formulation (17) is the numerical approximated version of the partition method presented in [3].

Among other methods presented in [3], another one is particularly interesting, especially due to its simplicity, and because of its better accuracy for finely discretized spheres. [3] called this method the 1-DP method. It is defined as:

$$\delta_{k,l} = \begin{cases} 1 & \text{for } l = \arg \max_{j \in \llbracket 1; N_d \rrbracket} \zeta(\mathbf{s}_k) \cdot \mathbf{s}_j \\ 0 & \text{else} \end{cases} \quad \forall k \in \llbracket 1; N_d \rrbracket. \quad (18)$$

In this strategy, for a given reflected direction, say \mathbf{s}_k , there is a single corresponding incident direction \mathbf{s}_l . However, a given incident direction, say \mathbf{s}_l , can give its energy to several reflected directions \mathbf{s}_k .

Another strategy -we denote as the modified 1-DP method, is defined as:

$$\delta_{k,l} = \begin{cases} 1 & \text{for } k = \arg \max_{j \in \llbracket 1; N_d \rrbracket} \zeta(\mathbf{s}_l) \cdot \mathbf{s}_j \\ 0 & \text{else} \end{cases} \quad \forall l \in \llbracket 1; N_d \rrbracket. \quad (19)$$

In this strategy, for a given incident direction, say \mathbf{s}_l , there is a single corresponding reflected direction \mathbf{s}_k . However, a given reflected direction, say \mathbf{s}_k can receive its energy from several incident directions \mathbf{s}_l .

2.3. Balls and spheres

From the previous section it is seen that most integrals are to be performed over the unit sphere. However, within the context of finite elements, it can be advantageous to rather perform integrals over the unit ball. The main reasons come from the following remark.

Remark 3. If a finite element domain specific language (DSL) (such as [29, 30, 31], to cite but a few) is used to build these matrices, integrations over the unit sphere may be difficult to implement, the reason being that \mathcal{S}^2 contains 3 components in a Cartesian coordinate system, rather than just 2 components.

Definition 1 (Sphere). The unit sphere for the dimension 3 is defined as

$$\mathcal{S}^2 = \{\mathbf{x} \mid \|\mathbf{x}\| = 1\}.$$

Remark 4. For a n -dimensional problem, the unit sphere is $(n - 1)$ -dimensional. However, when expressed in a Cartesian system, its definition needs n ordinates. One has, for one-, two-, and three-dimensional problems, respectively:

$$\mathcal{S}^0 = \{(x_1) \mid x_1^2 = 1\}, \quad \mathcal{S}^1 = \{(x_1, x_2) \mid x_1^2 + x_2^2 = 1\}, \quad \mathcal{S}^2 = \{(x_1, x_2, x_3) \mid x_1^2 + x_2^2 + x_3^2 = 1\}.$$

So, for $n = 1$ the sphere reduces to the set of two points, for $n = 2$ the sphere reduces to the unit circle, and for $n = 3$ the sphere is the usual one.

Definition 2 (Ball). The closed unit ball for the dimension 3 is defined as

$$\mathcal{B}^3 = \{\mathbf{x} \mid \|\mathbf{x}\| \leq 1\}.$$

Remark 5. The boundary $\partial\mathcal{B}^3$ of the unit ball \mathcal{B}^3 is the surface \mathcal{S}^2 . Hence

$$\int_{\partial\mathcal{B}^3} \cdot d\mathbf{x} = \oint_{\mathcal{S}^2} \cdot d\mathbf{x}.$$

Definition 3 (Accompanying ball triangulation). Let \mathcal{S}_h^2 be the triangulation of the unit sphere, and \mathcal{B}_h^3 be a triangulation of the unit ball. \mathcal{B}_h^3 is said to be an accompanying ball triangulation of \mathcal{S}_h^2 if, and only if, all elements of \mathcal{S}_h^2 are boundary elements of \mathcal{B}_h^3 , and all boundary elements of \mathcal{B}_h^3 are elements of \mathcal{S}_h^2 .

Definition 4 (Restriction matrix). Based on the triangulation \mathcal{S}_h^2 , a finite element functional space expressed with polynomial functions of degree k can be built. Let us denote it $V_h(\mathcal{S}_h^2, \mathbb{P}_k)$. Also, let us denote \mathcal{N}_1 the corresponding set of indices of degrees of freedom. Further, based on the mesh \mathcal{B}_h^3 , a finite element functional space expressed with polynomial functions of degree k can also be built. Let us denote it $V_h(\mathcal{B}_h^3, \mathbb{P}_k)$, and let \mathcal{N} be the corresponding set of indices of degrees of freedom. Based on the definition of the dual triangulation, with \mathcal{N}_2 the set of indices of degrees of freedom respecting the partition $\mathcal{N} = \mathcal{N}_1 \cup \mathcal{N}_2$, the restriction operator can be defined. We use for that the same approach as for partitioning the unity function in domain decomposition: for a vector $\mathbf{u} \in \mathbb{R}^{\#\mathcal{N}}$, the restriction of this vector to the “boundary subdomain” can be expressed as $R_1\mathbf{u}$, where R_1 is a rectangular Boolean matrix of size $\#\mathcal{N}_1 \times \#\mathcal{N}$ defined such that $I_d = R_1^\top D_1 R_1 + R_2^\top D_2 R_2$, with D_i diagonal matrices of size $\#\mathcal{N}_i \times \#\mathcal{N}_i$, and I_d the identity matrix of size $\#\mathcal{N} \times \#\mathcal{N}$. See [32] for some examples.

Remark 6. The number $\#\mathcal{N}_1$ is, in fact, the number of discrete ordinates, i.e., N_d .

Remark 7. Definition 4 will be useful for mapping values from the ball \mathcal{B}_h^3 to the sphere \mathcal{S}^2 , as will be presented later on in algorithm 1.

The strategy presented here consists in building all vectors and matrices based on angular finite elements, the functional spaces being defined based on a ball mesh. Then, as a second step, the restriction matrix is used to extract adequate values only on boundaries, i.e. values related to the sphere discretization.

2.4. \mathbb{P}_0 angular finite element basis

Let the unit sphere \mathcal{S}^2 be discretized such that its approximation is the union of disjoint elements \mathcal{T}_j^h (the superscript h is hereafter omitted for readability considerations). The following properties hold, for the particular case of \mathbb{P}_0 finite element space:

- test functions $\varphi_i(s \in \mathcal{T}_j) = \delta_{i,j}$, which is 1 if $j = i$ and 0 elsewhere;
- the intersection of the support for $\varphi_i^s(\mathbf{s})$ and $\varphi_j^s(\mathbf{s})$ is null as soon as $i \neq j$;
- the direction \mathbf{s} is constant over the whole element \mathcal{T}_j ;
- the directions to be considered $\mathbf{s}_k = (x_k, y_k, z_k)^\top$, $k = 1, \dots, N_d$ are judiciously chosen to be barycenters:

$$x_k = \int_{\mathcal{T}_k} x \, d\mathbf{s} ; y_k = \int_{\mathcal{T}_k} y \, d\mathbf{s} ; z_k = \int_{\mathcal{T}_k} z \, d\mathbf{s}. \quad (20)$$

The normalization $\|\mathbf{s}_k\|_2 = 1$ is then to be performed following remark 2.

From these properties, one has, for $i \neq j$:

$$\int_{\mathcal{S}^2} \varphi_i^s(\mathbf{s}) \varphi_j^s(\mathbf{s}) \mathbf{s}_\alpha \, d\mathbf{s} = 0 \quad ; \quad \int_{\mathcal{S}^2} \varphi_i^s(\mathbf{s}) \varphi_j^s(\mathbf{s}) \, d\mathbf{s} = 0, \quad (21)$$

which is equivalent to

$$\overline{\mathcal{A}^\alpha} = 0 \quad ; \quad \overline{\mathcal{B}} = 0. \quad (22)$$

Otherwise, for $i = j$, one has:

$$\int_{\mathcal{S}^2} \varphi_j^s(\mathbf{s}) \varphi_j^s(\mathbf{s}) \mathbf{s}_\alpha \, d\mathbf{s} \approx (\mathbf{s}_\alpha)_j \int_{\mathcal{T}_j} d\mathbf{s} = (\mathbf{s}_\alpha)_j |\mathcal{T}_j^s|, \quad (23)$$

which is equivalent to

$$\mathcal{A}_{j,j}^\alpha = |\mathcal{T}_j^s| (\mathbf{s}_\alpha)_j \quad ; \quad \mathcal{B}_{j,j} = |\mathcal{T}_j^s|. \quad (24)$$

Besides, the term related to the scattering operator is derived this way:

$$\begin{aligned} \int_{\mathcal{S}^2} \varphi_i(\mathbf{s}) \, d\mathbf{s} \int_{\mathcal{S}^2} \phi(\mathbf{s}, \mathbf{s}_i) \varphi_j(\mathbf{s}) \, d\mathbf{s} &= \int_{\mathcal{T}_i} \varphi_i(\mathbf{s}) \, d\mathbf{s} \int_{\mathcal{T}_j} \phi(\mathbf{s}, \mathbf{s}_i) \varphi_j(\mathbf{s}) \, d\mathbf{s} \\ &= |\mathcal{T}_i^s| \int_{\mathcal{T}_j} \phi(\mathbf{s}, \mathbf{s}_i) \, d\mathbf{s}. \end{aligned} \quad (25)$$

Finally, the linear term is given by:

$$\int_{\mathcal{S}^2} \varphi_j^s(\mathbf{s}) \, d\mathbf{s} = \int_{\mathcal{T}_j^s} d\mathbf{s} = |\mathcal{T}_j^s|. \quad (26)$$

Gathering all components gives:

$$|\mathcal{T}_j^s| \mathbf{s}_j \cdot \nabla \mathbf{I}_j + (\kappa + \sigma_s) |\mathcal{T}_j^s| \mathbf{I}_j - \sigma_s \sum_i |\mathcal{T}_i^s| \int_{\mathcal{T}_j} \phi(\mathbf{s}, \mathbf{s}_i) \, d\mathbf{s} \mathbf{I}_i - |\mathcal{T}_j^s| \kappa I_b = 0 \quad \forall j. \quad (27)$$

Remark 8. Considering that the phase function $\phi(\mathbf{s}, \mathbf{s}_i)$ does not vary much within the cell \mathcal{T}_j , the previous component can be approximated to:

$$\int_{\mathcal{S}^2} \varphi_i(\mathbf{s}) \, d\mathbf{s} \int_{\mathcal{S}^2} \phi(\mathbf{s}, \mathbf{s}_i) \varphi_j(\mathbf{s}) \, d\mathbf{s} \approx |\mathcal{T}_i^s| \phi(\mathbf{s}_j, \mathbf{s}_i) \int_{\mathcal{T}_j} d\mathbf{s} = |\mathcal{T}_i^s| \phi(\mathbf{s}_i, \mathbf{s}_j) |\mathcal{T}_j^s|. \quad (28)$$

The measure $|\mathcal{T}_j^s|$ being in factor of all terms, we arrive to:

$$\mathbf{s}_j \cdot \nabla \mathbf{I}_j + (\kappa + \sigma_s) \mathbf{I}_j - \sigma_s \sum_i |\mathcal{T}_i^s| \phi(\mathbf{s}_i, \mathbf{s}_j) \mathbf{I}_i - \kappa I_b = 0 \quad \forall j. \quad (29)$$

Remark 9. Considering the approximation (28) used for the \mathbb{P}_0 FEM, (27) yields (29), which is exactly equivalent to the formulation given by a discrete ordinate method when this one is based on the sphere discretization (i.e. based on a variational formulation), as defined for example in [5]). Note that such a method is totally different from standard quadratures, such as S_n for example, [25, 2, 33].

3. Ad hoc angular discretization

The main ingredients for angular finite elements were introduced in the previous section, and the mesh adaptation of the unit sphere is now dealt with. Since it is our intention to be able to deal with radiation transport in both scattering and non-scattering media, both with and without reflection on boundaries, some crucial choices have to be done as a prerequisite.

First, when a Lagrange functional space $\mathbb{P}_{k>0}$ is chosen, the matrices \mathcal{A}^α and \mathcal{B} previously defined by (10), though being sparse by nature, still contain some non-null components out of the diagonal (approximately 5 to 6 for $k = 1$). Such non-null components artificially add a coupling of the radiative intensity between different directions, as the scattering matrix \mathcal{C} does. So, when dealing with non-scattering media or low scattering media, and when specular reflection is dealt with, then the \mathbb{P}_0 Lagrange functional space should be preferred to any $\mathbb{P}_{k>0}$, in order to avoid such artificial coupling.

Secondly, the mesh adaptation process is based on the computation of a metric. A discrete approximation of the metric uses the mesh as a support. In general, the metric is defined on the vertices of the mesh rather than on the elements themselves [34]. One of the reasons is that, from the knowledge of a metric \mathcal{M} defined on vertices, its continuous version

can be given thanks to an interpolation scheme. So, from the knowledge of the metric on vertices, its gradient can be derived, with

$$\nabla \mathcal{M}(\mathbf{s}) = \sum_{i=1}^{N_d} \nabla \varphi_i(\mathbf{s}) \mathcal{M}(\mathbf{s}_i). \quad (30)$$

The following two arguments justify the introduction of a vertex-based \mathbb{P}_0 finite element space: i) a \mathbb{P}_0 finite element space is to be chosen for the angular finite element scheme if collimated radiation is dealt with, or when considering small scattering problems, and, ii) the metric is preferably defined on vertices. Let us denote it as $\mathbb{P}_{0,v}$, and explain in the next section how it is constructed in an efficient way, and how it is used in the angular discretization process.

3.1. Vertex-based $\mathbb{P}_{0,v}$ finite elements

Given a triangulation \mathcal{S}_h^2 of the unit sphere, a vertex-based \mathbb{P}_0 finite element space is based on another triangulation, $\widetilde{\mathcal{S}}_h^2$, dual of \mathcal{S}_h^2 , such that $\mathbb{P}_{0,v}(\mathcal{S}_h^2) = \mathbb{P}_0(\widetilde{\mathcal{S}}_h^2)$. Figure 1 schematically presents this construction. The primal triangulation \mathcal{S}_h^2 , presented in the middle, is composed of triangular cells and vertices. Each cell of \mathcal{S}_h^2 can be divided into three polygons of equal area considering the three lines passing by its barycenter and the three middle edge points. Each polygon is thus closed by one vertex from the primal triangulation, the barycenter of the parent cell of the primal triangulation, and two more points in middle edges of the parent cell of the primal triangulation. The union of all polygons forms the dual triangulation $\widetilde{\mathcal{S}}_h^2$. A dual triangulation is presented in the left-hand-side of figure 1. Each vertex of the primal triangulation lies within a cell of the dual triangulation. Now, a \mathbb{P}_0 finite element space can be defined on $\widetilde{\mathcal{S}}_h^2$. Defining for the $\mathbb{P}_0(\widetilde{\mathcal{S}}_h^2)$, $\tilde{\varphi}_i(\mathbf{s} \in \mathcal{T}_j) = \delta_{i,j}$, the weights are calculated through this integration:

$$\omega_i = \int_{\widetilde{\mathcal{S}}_h^2} \tilde{\varphi}_i(\mathbf{s}) \, d\mathbf{s}. \quad (31)$$

Alternatively, denoting $\mathcal{T}_j^{(i)}$ the elements $\mathcal{T}_j \in \mathcal{S}_h^2$ whose the node P_i is a vertex of it, then the weight associated to this vertex P_i is the sum over all triangular neighbors of one third of their related area:

$$\omega_i = \sum_j \frac{1}{3} |\mathcal{T}_j^{(i)}|. \quad (32)$$

But it is also possible to compute the weights ω_i without building explicitly the dual triangulation useful for (31), or through a discrete summation as in (32). Defining $\{\varphi_j(\mathbf{s})\}_{j=1}^{N_d}$ as a basis of continuous Lagrange linear functions (\mathbb{P}_1 functions) defined on the primal triangulation, we have, by construction:

$$\omega_i = \int_{\mathcal{S}_h^2} \varphi_i(\mathbf{s}) \, d\mathbf{s}. \quad (33)$$

This property is interesting because the weights ω_i can be computed from a single integration using any finite element library.

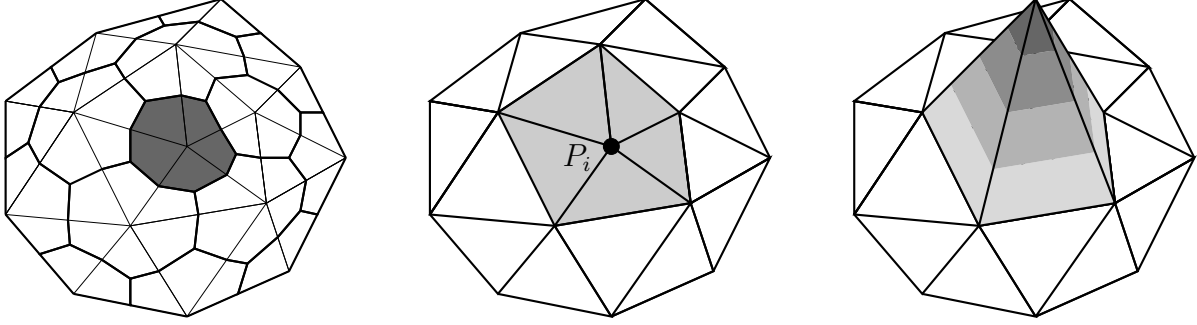


Figure 1: Triangulations \mathcal{S}_h^2 and $\widetilde{\mathcal{S}}_h^2$ along with \mathbb{P}_0 and \mathbb{P}_1 finite element spaces. Left: triangulation $\widetilde{\mathcal{S}}_h^2$; the mesh is composed of polygons, and the \mathbb{P}_0 space is considered. Middle: triangulation \mathcal{S}_h^2 : the mesh is composed of triangular cells, and the \mathbb{P}_0 space is considered. Right: triangulation \mathcal{S}_h^2 : the mesh is composed of triangular cells, and the \mathbb{P}_1 space is considered. The area represented by the gray surface in the left sub-figure is equal to one third of the area represented by the gray surface in the middle sub-figure, which is also equal to the volume represented schematically in the right sub-figure.

3.2. Adaptation

In this article, the adaptation process itself uses the open source library mmglib available from the Mmg platform [35] which follows the theoretical results given in [34, 36].

At each iteration, one has first to extract some space-independent value out of the radiative computation, and let us denote it $\mathcal{I}(\mathbf{s}_i)$, $\forall i \in \llbracket 1; N_d \rrbracket$. Many quantities could be useful. For example, the results presented in the numerical results section are built with the global intensity defined by:

$$\mathcal{I}(\mathbf{s}_i) = \int_{\mathcal{D}} I(\mathbf{x}, \mathbf{s}_i) \, d\mathbf{x}. \quad (34)$$

Then, from the knowledge of the set of space-independent outputs $\{\mathcal{I}(\mathbf{s}_i)\}_{i=1}^{N_d}$, one can compute its gradient $\mathbf{G}(\mathbf{s}_i) = \nabla_s \mathcal{I}(\mathbf{s}_i)$, if $\mathcal{I}(\mathbf{s}_i)$, is defined in a \mathbb{P}_1 finite element functional space, for example, and also approximate its Hessian $\mathbf{H}(\mathbf{s}_i) = \nabla_s^2 \mathcal{I}(\mathbf{s}_i)$. Note that among other methods for the approximation of the Hessian, such as the finite element method [37] or the use of the Green formulation [38], the method based on the Taylor development associated to the solution of a linear system has been preferred by the developers of the used mmglib library [34]. More precisely, for $\hat{\mathbf{s}}$ connected with \mathbf{s}_i , one writes:

$$\mathcal{I}(\mathbf{s}_i) = \mathcal{I}(\hat{\mathbf{s}}) + \overrightarrow{\hat{\mathbf{s}}\mathbf{s}_i} \cdot \mathbf{G}(\hat{\mathbf{s}}) + \frac{1}{2} \overrightarrow{\hat{\mathbf{s}}\mathbf{s}_i} \cdot \mathbf{H}(\hat{\mathbf{s}}) \overrightarrow{\hat{\mathbf{s}}\mathbf{s}_i}. \quad (35)$$

In the case of a \mathbb{P}_1 finite element space defined for \mathcal{I} , its error of interpolation, ϵ over elements is directly related to this Hessian. An over-determined system with 6 unknowns is to be solved to get the Hessian. The isotropic metric is then given by the following diagonal matrix

$$\mathcal{M}_{i,i} = \bar{\lambda}, \text{ and } \mathcal{M}_{i,j \neq i} = 0. \quad (36)$$

with $\bar{\lambda} = \max_{i=1,2,3} \tilde{\lambda}_i$, in which, for a given i , $\tilde{\lambda}_i$ depends on the eigenvalue λ_i of the related Hessian \mathbf{H} , as well as some user-defined parameters, such as the minimum size h_{\min} and the

maximum size h_{\max} of the related element, a theoretical constant value c , and a tolerance value ϵ_{tol} specified by the user [34]:

$$\tilde{\lambda}_i = \min \left(\max \left(\frac{c|\lambda_i|}{\epsilon_{\text{tol}}}, \frac{1}{h_{\max}^2} \right), \frac{1}{h_{\min}^2} \right). \quad (37)$$

The metric, which is a diagonal matrix, is defined on each vertex of the unit ball. This constitutes the input for the mesh adaptation process. If \mathbf{s}_i is a vertex and $\mathcal{M}(\mathbf{s}_i)$ is the metric on this vertex, the process consists in building a new mesh such that all edges $\mathbf{e}_i = \mathbf{s}_i \hat{\mathbf{s}}$ are of unit length in their metric:

$$l_{\mathcal{M}(\mathbf{s}_i)}(\mathbf{s}_i \hat{\mathbf{s}}) = (\overrightarrow{\mathbf{s}_i \hat{\mathbf{s}}}, \overrightarrow{\mathbf{s}_i \hat{\mathbf{s}}})_{\mathcal{M}(\mathbf{s}_i)}^{\frac{1}{2}} = 1. \quad (38)$$

Note that a detailed description of this technical process is far beyond the scope of this paper and that the external library mmglib optimizes this distribution of vertices when given a metric map.

Algorithm 1 gives the main features of the angular adaptivity. The process is iterative. Starting from a discretized unit ball $\mathcal{B}_h^{(k)}$, the discretized unit sphere $\mathcal{S}_h^{(k)}$ is extracted from it, see section 2.3. The weights associated to the discrete ordinates \mathbf{s}_i , $i \in \llbracket 1; N_d \rrbracket$ are then updated, see section 2.1, along with the partition ratio coefficients useful for modeling specular reflection, see section 2.2. The fully discretized problem is then solved, see next section. A space-independent variable is then computed out of the solution, and a metric is evaluated. Finally, the mesh is adapted from the metric. The full process is schematically given in Algorithm 1.

Algorithm 1: Angular adaptation procedure.

Input : $\mathcal{B}^{(0)}$

while $\epsilon > \epsilon_{\text{tol}}$ and $k < k_{\max}$ **do**

1. extract the unit sphere $\mathcal{S}_h^{(k)}$ from $\mathcal{B}_h^{(k)}$;
2. compute angular discretization matrices;
3. compute spatial discretization matrices (finite elements);
4. solve the RTE;
5. output an angular-only-dependent variable, e.g. $\mathcal{I}(\mathbf{s}_i) = \int_{\mathcal{D}} I(\mathbf{x}, \mathbf{s}_i) d\mathbf{x}$;
6. project \mathcal{I} onto the ball thanks to the Dirichlet elliptic problem $-\Delta \mathcal{J}(\mathbf{s}) = 0$, $\mathcal{J}(\partial \mathcal{B}^{(k)}) = \mathcal{I}$;
7. evaluation of the metric \mathcal{M} on the ball $\mathcal{B}^{(k)}$, based on \mathcal{J}_i ;
8. adaptation of the ball $\mathcal{B}^{(k)}$ based on the metric \mathcal{M}_i ;
9. $k \leftarrow k + 1$;

end

Output: adapted angular discretization $\hat{\mathcal{S}} = \mathcal{S}^{(k)}$.

4. Vectorial finite elements for spatial discretization

Using $\omega_m = |\mathcal{T}_m^s|$ and $\Phi_{m,n} = \phi(\mathbf{s}_m, \mathbf{s}_n)$, the radiative transfer problem represented by Eq. (29) can be transformed into the following system of semi-discretized equations:

$$\forall m = 1, \dots, N_d : \quad (\mathbf{s}_m \cdot \nabla + \beta(\mathbf{x})) I_m(\mathbf{x}) - \sigma_s(\mathbf{x}) \sum_{n=1}^{N_d} \omega_n I_n(\mathbf{x}) \Phi_{m,n} = \kappa(\mathbf{x}) I_b(\mathbf{x}), \quad (39)$$

here β represents the extinction coefficient of the medium: $\beta = \kappa + \sigma_s$.

In a finite element context, this problem consists in searching a vector of radiative intensities \mathbb{I} using an appropriate vectorial test function \mathbb{V} which lies in the corresponding vectorial functional space $\mathcal{W}^{N_d} = \prod_{i=1}^{N_d} \mathcal{V}^i$ (see [9] for more information on that point). Let us define:

$$\mathbb{I} = \begin{pmatrix} I_1 \\ I_2 \\ \vdots \\ I_{N_d} \end{pmatrix} ; \quad \mathbb{S} = \begin{pmatrix} \mathbf{s}_1 \\ \mathbf{s}_2 \\ \vdots \\ \mathbf{s}_{N_d} \end{pmatrix} ; \quad \mathbb{V} = \begin{pmatrix} v_1 \\ v_2 \\ \vdots \\ v_{N_d} \end{pmatrix}. \quad (40)$$

$$\Theta = \begin{pmatrix} \sigma_s \omega_1 \phi_{1,1} & \sigma_s \omega_2 \phi_{1,2} & \cdots & \sigma_s \omega_{N_d} \phi_{1,N_d} \\ \sigma_s \omega_1 \phi_{2,1} & \sigma_s \omega_2 \phi_{2,2} & \cdots & \sigma_s \omega_{N_d} \phi_{2,N_d} \\ \vdots & \vdots & \ddots & \vdots \\ \sigma_s \omega_1 \phi_{N_d,1} & \sigma_s \omega_2 \phi_{N_d,2} & \cdots & \sigma_s \omega_{N_d} \phi_{N_d,N_d} \end{pmatrix}. \quad (41)$$

Using these notations, we can rewrite the semi-discretized equation (39) in its vectorial form as

$$\mathbb{S} \cdot \nabla \mathbb{I} + \beta \mathbb{I} - \Theta \mathbb{I} = \kappa I_b \mathbb{1}, \quad (42)$$

with $\mathbb{1}$ being the identity vector of same order as \mathbb{I} . Here, $\mathbb{S} \cdot \nabla \mathbb{I}$ would give a vector, the i th component of which will be given by $(\mathbb{S} \cdot \nabla \mathbb{I})_i = \mathbf{s}_i \cdot \nabla I_i$. We also introduce the following notations: $\mathbb{A}^\top \mathbb{B} = \sum_i \mathbb{A}_i \mathbb{B}_i$ and $(\mathbb{A} : \mathbb{B})_i = \mathbb{A}_i \mathbb{B}_i$, for the sake of conciseness.

The vectorial finite element-based SUPG weak formulation can now be built by multiplying the vectorial equation (42) with a vectorial test function $\mathbb{V} + \gamma \mathbb{S} \cdot \nabla \mathbb{V}$, then integrating over the domain of interest \mathcal{D} . Based on that, the problem now reads:

search $\mathbb{I} \in \mathcal{W}^{N_d}$ that satisfies:

$$\begin{aligned} & \int_{\mathcal{D}} (\mathbb{S} \cdot \nabla \mathbb{I} + \beta \mathbb{I})^\top (\mathbb{V} + \gamma \mathbb{S} \cdot \nabla \mathbb{V}) \, d\mathbf{x} - \int_{\mathcal{D}} (\Theta \mathbb{I})^\top (\mathbb{V} + \gamma \mathbb{S} \cdot \nabla \mathbb{V}) \, d\mathbf{x} \\ & = \int_{\mathcal{D}} (\kappa I_b \mathbb{1})^\top (\mathbb{V} + \gamma \mathbb{S} \cdot \nabla \mathbb{V}) \, d\mathbf{x} \quad \forall \mathbb{V} \in \mathcal{W}^{N_d}. \end{aligned} \quad (43)$$

The Green theorem is then applied, so that the problem becomes:

$$\begin{aligned}
& \text{search } \mathbb{I} \in \mathcal{W}^{N_d} \text{ that satisfies:} \\
& - \int_{\mathcal{D}} (\mathcal{S} \cdot \nabla \mathbb{W})^\top \mathbb{I} \, d\mathbf{x} + \int_{\partial \mathcal{D}} (\mathcal{S} \cdot \mathbf{n} : \mathbb{H}_{[\mathcal{S} \cdot \mathbf{n} > 0]} : \mathbb{I})^\top \mathbb{V} \, d\mathbf{x} \\
& + \int_{\partial \mathcal{D}} (\mathcal{S} \cdot \mathbf{n} : \mathbb{H}_{[\mathcal{S} \cdot \mathbf{n} < 0]} : \mathbb{I}_{\text{in}})^\top \mathbb{V} \, d\mathbf{x} + \int_{\mathcal{D}} (\mathcal{S} \cdot \nabla \mathbb{I})^\top (\gamma \mathcal{S} \cdot \nabla \mathbb{W}) \, d\mathbf{x} \\
& + \int_{\mathcal{D}} (\beta \mathbb{I})^\top (\mathbb{V} + \gamma \mathcal{S} \cdot \nabla \mathbb{W}) \, d\mathbf{x} - \int_{\mathcal{D}} (\Theta \mathbb{I})^\top (\mathbb{V} + \gamma \mathcal{S} \cdot \nabla \mathbb{W}) \, d\mathbf{x} \\
& = \int_{\mathcal{D}} (\kappa I_b \mathbb{1})^\top (\mathbb{V} + \gamma \mathcal{S} \cdot \nabla \mathbb{W}) \, d\mathbf{x} \quad \forall \mathbb{V} \in \mathcal{W}^{N_d}.
\end{aligned} \tag{44}$$

Note that the vectorial indicator (Heaviside) function $\mathbb{H}_{[\mathcal{S} \cdot \mathbf{n} > 0]}$ has been introduced. This function results in zeros and ones depending on Boolean operations, e.g., $(\mathbb{H}_{[\mathcal{S} \cdot \mathbf{n} > 0]})_i$ equals one if and only if $\mathbf{s}_i \cdot \mathbf{n} > 0$, and zero elsewhere. Note also that the system (44) is a single equation while we have N_d equations with traditional finite elements, see [9] for more explanations on the subject.

Further, based on the triangulated spatial domain \mathcal{D} , a family of basis functions $\varphi(\mathbf{x}) \in \mathcal{V}_h$ is introduced such that $\mathbb{I} \approx \sum_{i=1}^N \mathbb{I}^i \varphi_i(\mathbf{x})$. This approximation then reduces the vectorial equation (44) to a linear system $AI = b$. The linear system then needs to be solved in order to realize the radiative intensity field \mathbb{I} .

5. Numerical applications

The proposed algorithm presented in previous sections is now tested numerically, in terms of accuracy respectively to a given angular discretization, i.e. a given number of discrete ordinates. More particularly, the (vectorial) DOM-FEM solver developed in [9] is used as reference. It will be shown, thanks to several examples, that the ad hoc scheme based on the $\mathbb{P}_{0,v}$ discretization yields much better accuracy with much fewer discrete ordinates to be used. Section 5.1 and section 5.2 start with two academic cases in which the construction of an ad hoc angular discretization yields superior performance than the ordinary DOM. Then, in section 5.3, the numerical modeling of the radiation propagation within a complex geometry with curved boundaries is dealt with. Such a configuration mimics a real-life engineering system.

5.1. Test 1: specular reflection only

An external collimated laser beam enters a three-dimensional non-scattering, non-absorbing medium. This beam is reflected upon a flat surface whose angle with respect to the primary beam is perfectly known. The reflected secondary beam is thus also known theoretically, and the closest direction involved in the set of discrete ordinates is chosen for the propagation of the secondary reflected beam, for the numerical simulation. As such, we can compare the numerical solution to the theoretical one. Note that in these simulations, as in all following ones, when the specular reflection is dealt with, the modified 1-DP method based on Eq. (19)

is the chosen strategy. However, one should note that the specular reflections handled with the partition method, equation (17), is totally compatible with the ad hoc angular adaptivity algorithm developed in this paper.

The three-dimensional geometry is an extruded deformed square defined by these vertices: $(0, 0, \pm h)$ m, $(1, 0, \pm h)$ m, $(1, 1, \pm h)$ m and $(0, (1 + 15\pi/72), \pm h)$ m. The width h is 0.1. The collimated laser beam enters in the boundary $x = 0$, on the y -range $[0.4 : 0.6]$, for the whole z -range. The direction of propagation is set to $(\sqrt{2}, \sqrt{2}, 0)$. Both absorption and scattering properties are set to zero, so that only the specular reflection is dealt with, added to the transport process.

Figure 2 presents the solutions, in terms of the radiative density $G(\mathbf{x}) = \int_{S^2} I(\mathbf{x}, \mathbf{s}) \, d\mathbf{s}$, for the DOM. It is seen that, for the first octahedral refinement (top subfigure), the incident beam is simply reflected back, because of the very low number of discrete ordinates. This of course yields large errors between the numerical solution and the theoretical one. Then, for more refined discretizations, the number of discrete ordinates is high enough, and the numerical solution approaches the theoretical solution.

Figure 3 then presents the solutions for the ad hoc $\mathbb{P}_{0,v}$ angular discretizations. It can be seen that the refinement of the mesh of the sphere is not uniform at all. Rather, the refinement is performed around the theoretical direction of reflection, i.e., the reflected beam. In fact, the refinement is present in the useful dominant direction of propagation.

The construction of such a non uniform discretization goes against what is generally admitted concerning the moments condition which usually need to be satisfied. However, note that, for the considered case, the specular reflection is the only physics that occurs. Recalling the definition of the moment of order p , for a given direction \mathbf{n} , as: $\mathcal{M}^{(p)} = \int_{S^2} (\mathbf{s} \cdot \mathbf{n})^p \, d\mathbf{s}$, one has, as a general rule, $\mathcal{M}^{(2p+1)} = 0$ and $\mathcal{M}^{(2p)} = \frac{4\pi}{2p+1}$ [20]. In our case, $\mathcal{M}^{(0)}$ is satisfied by construction, with the angular FEM. However, the rule for $p = 1$, shown by [39] to be important in determining the flux at a surface, is not really satisfied, and the diffusion condition for $p = 2$ cannot be satisfied either. The non conservation of the moments, present for this first test case, will be also present in the following cases, because non uniform discretizations are sought for intended use.

However, figure 4 presents, for this case, the evolution of the space-integrated error on the radiative density, as a function of the number of involved discrete ordinates, for both the DOM and the ad hoc $\mathbb{P}_{0,v}$ angular discretization. The error is calculated with:

$$e|_{L_2(\mathcal{D})}(G(\mathbf{x})) = \left(\int_{\mathcal{D}} \left(G(\mathbf{x}) - \hat{G}(\mathbf{x}) \right)^2 \, d\mathbf{x} \right)^{\frac{1}{2}}, \quad (45)$$

in which \hat{G} stands for the space-dependent theoretical radiative density. From this figure, it is seen that $N_d = 81$ discrete ordinates with the ad hoc discretization could give an error equal to 2.5×10^{-2} while $N_d = 512$ discrete ordinates is needed with the DOM to give the same error.

5.2. Test 2: absorbing and scattering medium impinged by a laser beam

In the previous subsection the angular adaptivity was tested for a pure reflecting problem with $\kappa = \sigma_s = 0$. To test the algorithm further, in this subsection we consider a problem

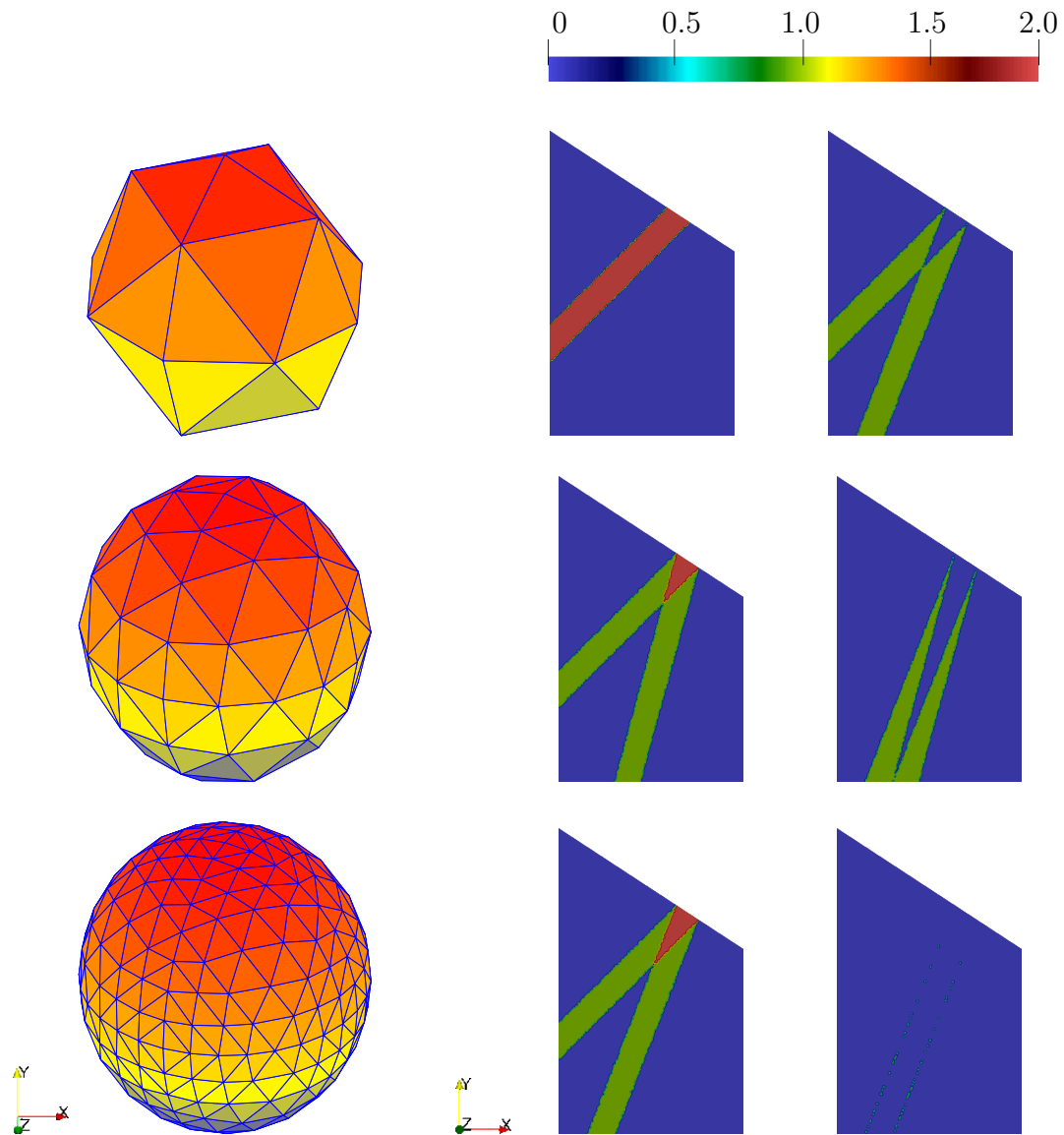


Figure 2: DOM-FEM. From top to bottom, N_d is, 32, 128, and 512, respectively. Left: sphere discretization. Middle: density on the plane $z = 0.15$. Right: absolute density error on the same plane $z = 0.15$.

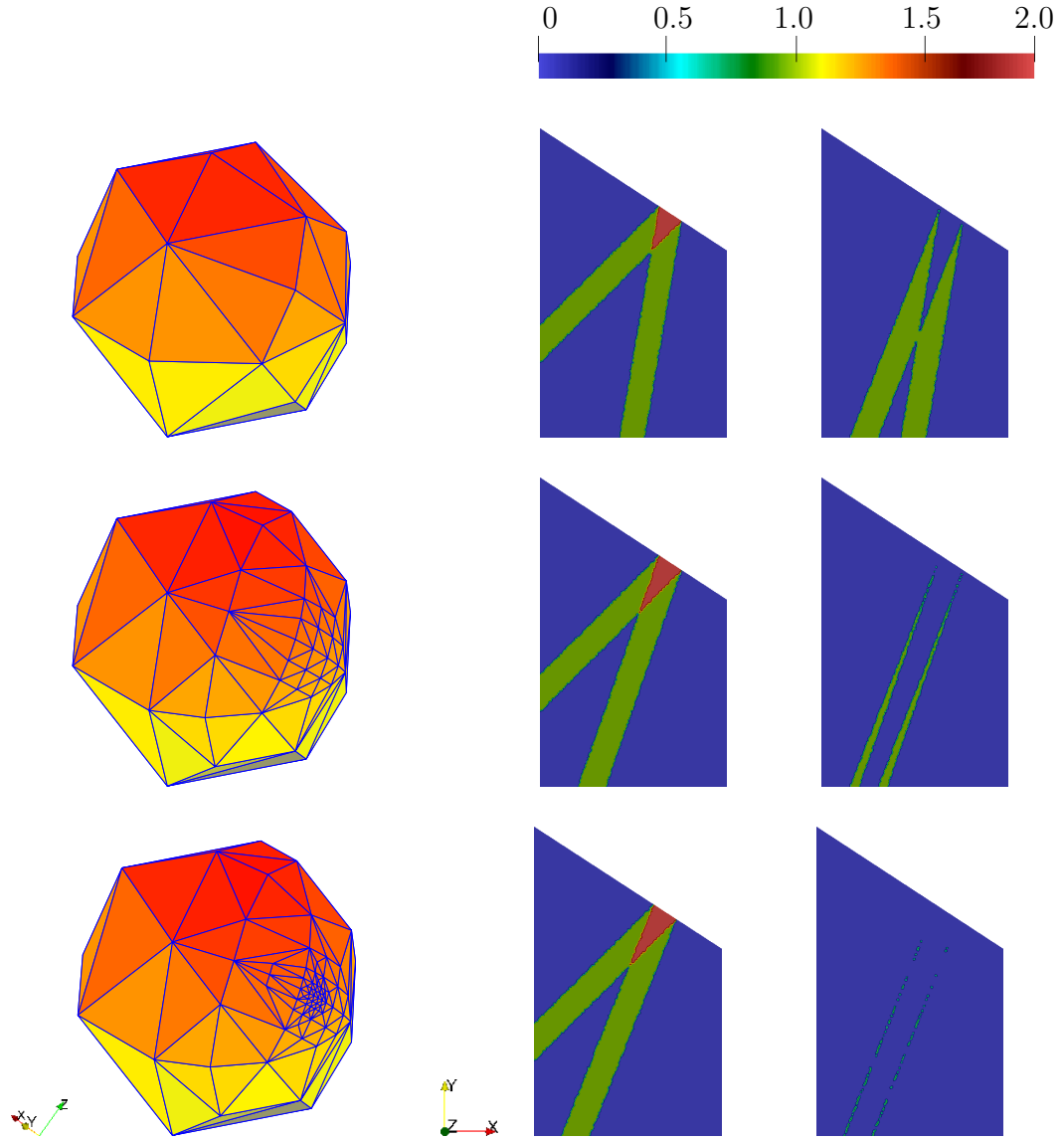


Figure 3: Ad hoc sphere discretizations based on the octahedron, with $\mathbb{P}_{0,v}$ angular finite elements. From top to bottom, N_d is, 22, 46, and 81. Left: sphere discretization. Middle: density on the plane $z = 0.15$. Right: absolute density error on the same plane $z = 0.15$.

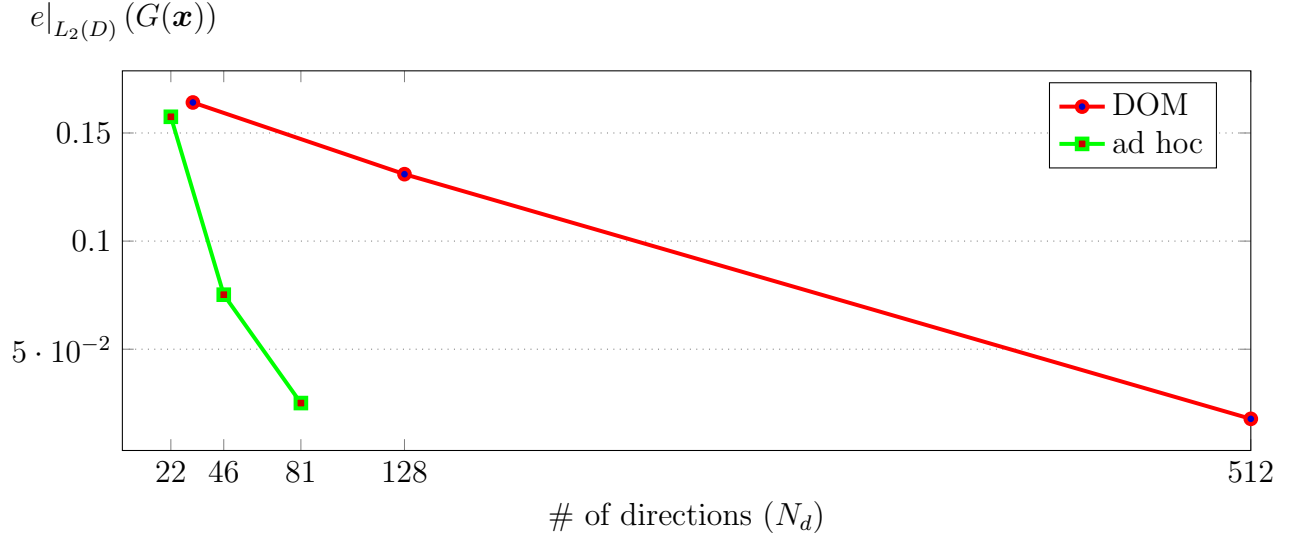


Figure 4: Evolution of the space-integrated error of the radiative density, as a function of involved discrete ordinates, for both uniform discretizations and ad hoc non-uniform discretizations.

composed by an absorbing, scattering, and reflecting medium.

The second test case concerns a collimated laser beam that impinges the center of one boundary of a geometry modeled by a cube of side length 1 cm. The source term follows a space-dependent exponential function given by:

$$I_{\text{in}} = \exp(-100 \times ((z - 0.5)^2 + (y - 0.5)^2)) \times \mathbb{1}_{((z-0.5)^2+(y-0.5)^2) \leq 0.1^2} \times \mathbb{1}_{(x=0)} \quad (46)$$

in which $\mathbb{1}_{(\text{boolean condition})}$ is equal to one, if and only if the boolean condition is satisfied, and zero otherwise. The medium is assumed to be absorbing, $\kappa = 0.1 \text{ cm}^{-1}$, and scattering, $\sigma = 5 \text{ cm}^{-1}$. The Henyey-Greenstein phase function is employed, with the anisotropy parameter $g = 0.2$.

Figure 5 presents the solution on a cut plane located in the middle of the z -length, in terms of the radiative density. From this figure it can be seen that the radiative density decreases while the photons travels within the medium, this is due to both the absorption and scattering effects. Note that this test is run on an ordinary laptop with 8 processors, using the domain decomposition method (the lighter blue contours present in Figure 5 represent the internal boundaries of the different domains). Note that such simulations have been highly studied and validated in previous papers [3, 10].

Figure 6 presents a series of ad hoc refined meshes of the unit sphere, starting from the first level of uniform refinement of the octahedron. The $\mathbb{P}_{0,v}$ angular finite element space is used. The associate number of degrees of freedom, N_d , is also given in the figure. It is seen that the angular refinement is concentrated around one particular direction, which is the dominant direction of propagation $(1, 0, 0)^\top$. At the very last level, the mesh is very fine around this direction only, and only 98 directions in total are involved.

One observes within the ad hoc refined meshes, figure 6, that the refinement occurs only in the forward half of the sphere. In other words, addition ordinates are created in the forward

half of the sphere, with the backward half of the sphere being unaltered. Moreover, one can also observe the clustering of ordinates around the primary direction (x axis). The placement of additional ordinates created for this problem adhere to the physics of the problem. Since the problem is forward scattering ($g = 0.2$), this explains the addition of ordinates in the forward half of the sphere, and since the problem contains a collimated source in the x axis, this leads to the dense clustering of ordinates around the x axis.

Figure 7 presents the error, in terms of radiative density, along two lines. The reference solution has been computed based on the ordinary uniform discretization involving 512 directions. From this figure, it can be seen that an ad hoc non uniform discretization can give discrepancies half of those obtained with a uniform discretization involving roughly the same amount of discrete ordinates (38 vs. 32). To go one step further, the next non uniform discretization involving 62 directions gives discrepancies of maximum 3 %. Next, both the uniform DOM scheme involving 128 ordinates and the ad hoc scheme with $\mathbb{P}_{0,v}$ angular FE scheme involving only 82 ordinates yield discrepancies of maximum 2 %.

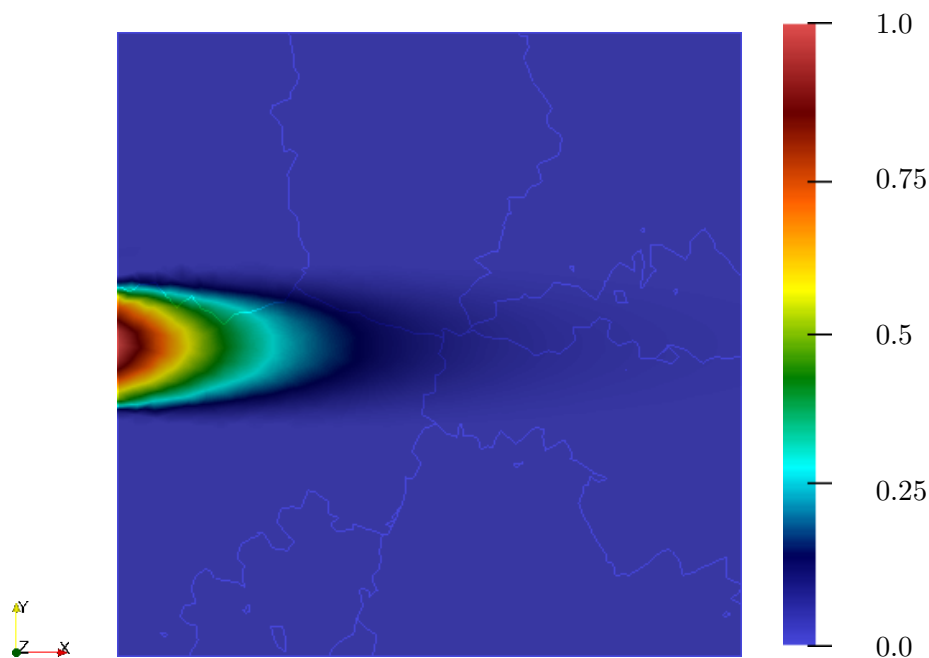


Figure 5: Reference density solution obtained with the octahedron discretization refined twice and \mathbb{P}_0 angular finite elements ($N_d = 128$).

5.3. Test 3: a complex geometry case

The test case involves the propagation of the radiation in vacuum bounded by curved boundaries which are partly reflecting. More particularly, we consider the reflection to be modeled by the specular contribution only with the reflectivity coefficient being equal to 0.2.

To detail the test case, assume a laser beam impinging both bottom and top material surfaces to be heated up. Due to the process of reflection, the computation of the radiative flux or the heat source does not follow a very straightforward trend. Simulations based on

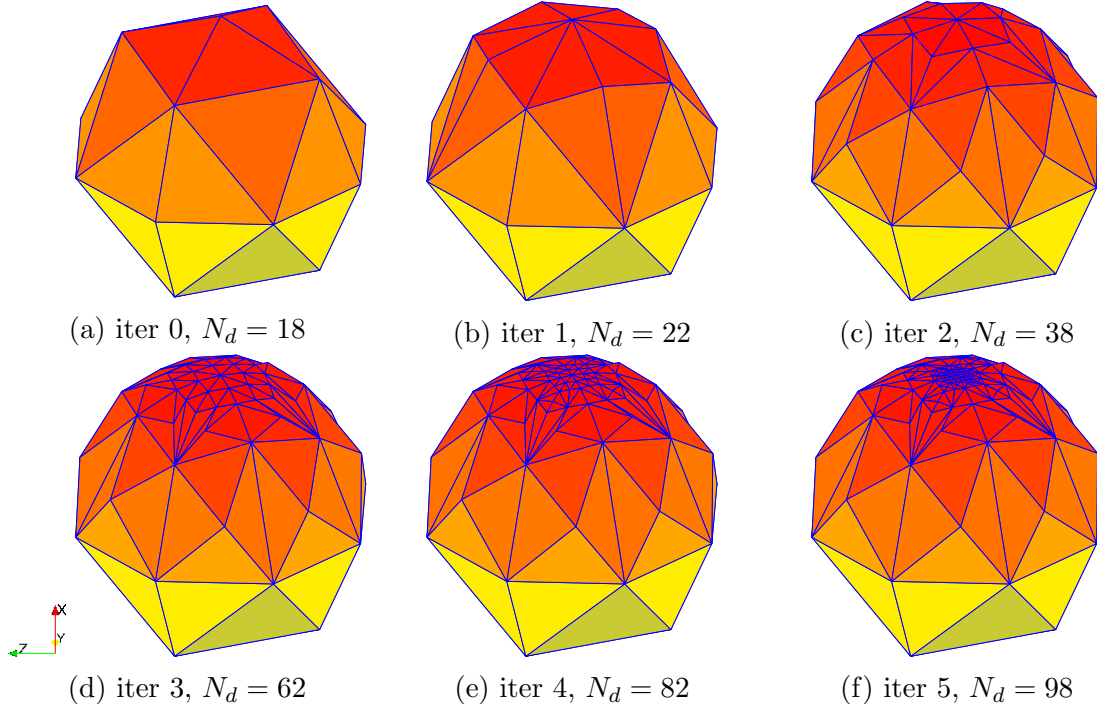


Figure 6: Ad hoc sphere discretizations of test case 2.

DOM-FEM would not be feasible without the process of adaptation of the angular discretization. The modeling difficulty comes essentially from the treatment of the specular reflection on the top boundary, because this one is curved. Indeed, even if this curved surface is very finely meshed, so that a high number of normals can be extracted from the mesh, the main difficulty concerns the angular discretization itself. Let us recall here briefly how it is implemented, much more explanations can be found in [3]. The unit sphere is discretized in a uniform way with a controlled size of patches. This $\hat{\mathcal{S}}_h^2$ gives a family of unit directions $\hat{\mathbf{s}}_i$, $i \in \llbracket 1; NN \rrbracket$. For a complex geometry with curved surfaces, NN typically exceeds thousands. Then, each unit outward normal extracted from the spatial mesh, say \mathbf{n}_k for a given surface element k , is replaced by its closest direction $\hat{\mathbf{s}}_i$, not for the radiative transfer computation itself, but for the specular reflection treatment explained in section 2.2, i.e., the application of Eq. (17), Eq. (18), or Eq. (19), according to the chosen strategy. Now, for the radiative transfer solver, the discretization of the unit sphere, say \mathcal{S}_h^2 cannot be that fine because of memory resource issues. For example, the triangulated $\hat{\mathcal{S}}_h^2$ could not be used instead of \mathcal{S}_h^2 . So, even though NN may be chosen big, N_d has to be limited to less than, say hundreds. In fact, for a uniform discretization, this amount N_d corresponds to quite a coarse discretization of the unit sphere, which does not permit accuracy of the modeling of the specular reflection on complex curved surfaces. This issue is the key point of this section.

Figures 8 and 9 present the solutions, in terms of the radiative density, for the DOM-FEM and for the adapted angular discretizations coupled with the $\mathbb{P}_{0,v}$ finite element space, respectively. The angular discretizations are presented in the left-hand-side, the related

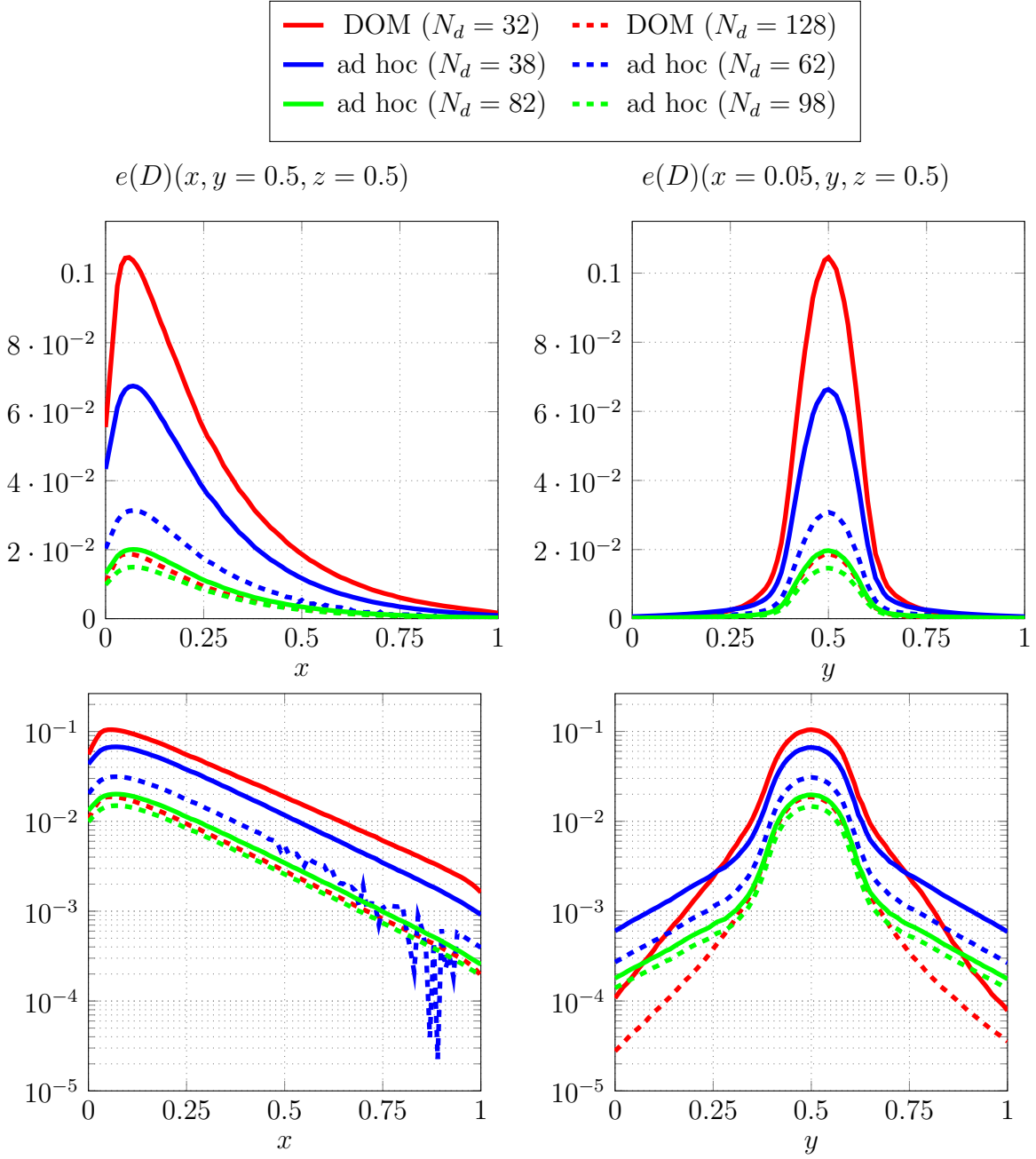


Figure 7: Error of the radiative density. The reference has been computed with the uniform angular discretization, and \mathbb{P}_0 angular finite elements ($N_d = 512$). Left: x -line for $y = 0.5$ and $z = 0.5$. Right: y -line for $x = 0.05$ and $z = 0.5$. The top figures use a linear scale for the y axis; the bottom figures use a log-10 scale for the y axis.

solutions on the cut plane ($x, y, z = 0$) are presented in the middle, and the related solutions on the bottom boundary ($x, y = 0, z$) are presented on right-hand-side. The radiative density entering from the left-hand-side boundary of the geometry is equal to one. Then, due to the process of reflection, the radiative density increases, reaching more than 1.4 close to the ending tip.

From Figure 8, it can be seen that, for all uniform discretizations, the density maps present some high discontinuities after the first reflection on the top boundary, like rays. This cannot be explained by any physical mean. Rather, this is due to the angular discretization which does not suit the physics, even for the finer discretization that involves 512 directions.

From Figure 9, it can be seen that such rays are also present for the adapted angular discretization, but only for the first levels. As in previous academic cases, the adaptation is performed such that the angular discretization is refined around dominant angles of propagation of the radiative intensity. In this case, dominant directions are, on the one hand, the reflected direction from the bottom boundary, and, on the other hand, a family of continuously reflected directions from the curved top boundary. After two iterations, the density maps are very smooth and do not present any strong discontinuity, with only 137 directions. At the next level, which involves only 201 directions, the density maps are very smooth, there is almost no discontinuity at all of the solution. The adaptation of the angular discretization could give a solution in accordance with the involved physics, even with a small number of directions.

6. conclusion

Based on angular vertex-based \mathbb{P}_0 finite elements, a methodology has been designed for angular adaptivity for solving the radiative transfer equation. The methodology has been designed for three-dimensional problems, as an extension to the two-dimensional problems previously presented in [1].

The algorithm is based on a posteriori calculations. The ad hoc angular discretization is obtained from an arbitrary sphere triangulation without any other predefined rule. The obtained ad hoc angular discretizations are optimized in such a way that they suit the particular physics under consideration.

Using comparative numerical tests based on the solution accuracy, the solutions provided by the obtained ad hoc discretizations are proven to be better than the ones provided by the standard uniform angular discretizations, increasing the finite element solution efficiency, i.e., the accuracy for a given number of discrete ordinates. Tests have been performed on absorbing and scattering media, with and without reflections on boundaries. All tested cases involved dominant directions of propagation, these cases being suited for such an optimization of the angular discretization.

The last test case involved a curved boundary on which reflection was involved. It could be shown that for the finer uniform DOM-FEM scheme involving 512 directions, the density maps presented some high discontinuities, like rays. This cannot be explained by any physical mean. Rather, this was due to the angular discretization which could not suit the physics.

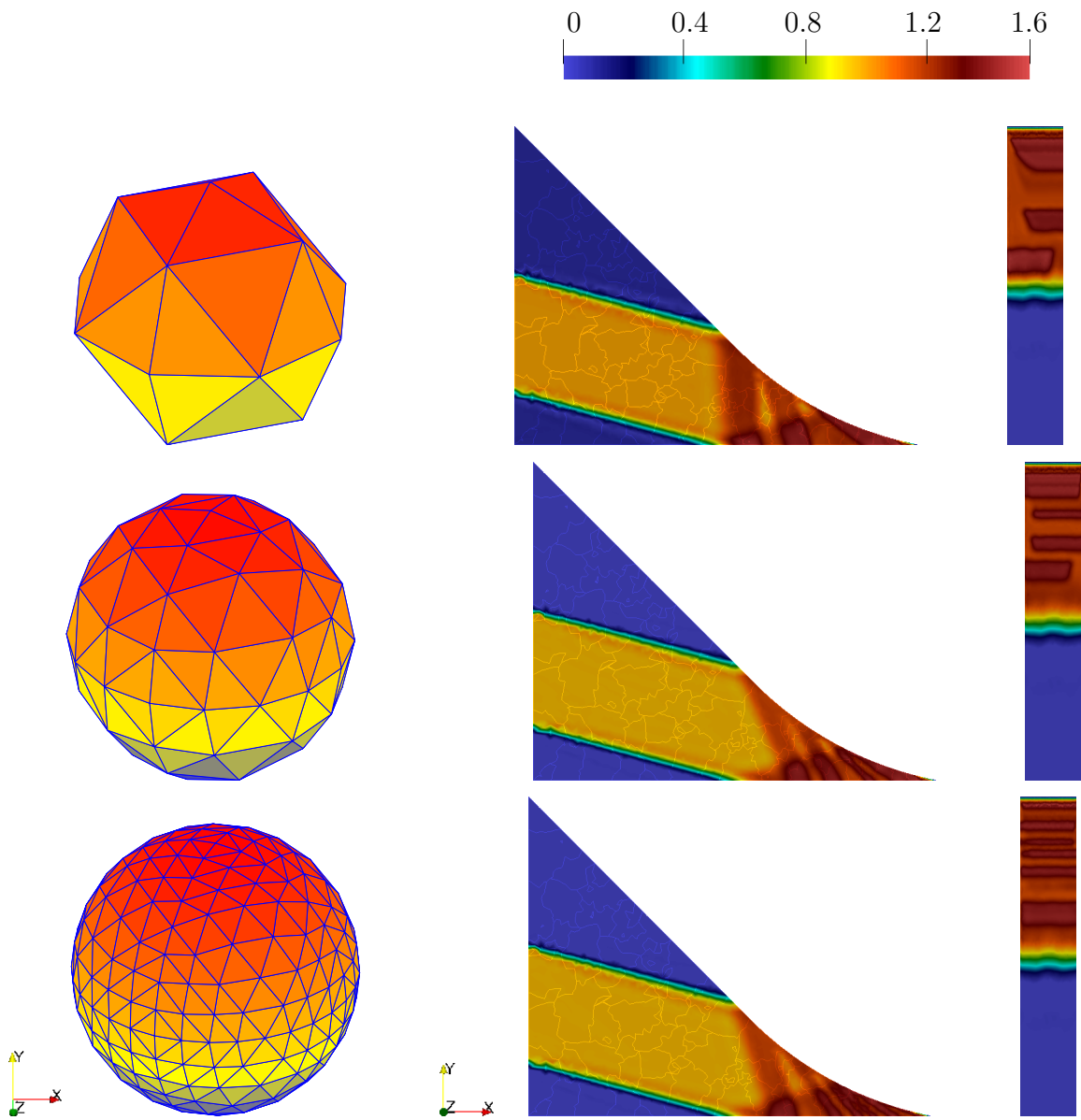


Figure 8: Uniform sphere discretization based on the octahedron, with \mathbb{P}_0 angular finite elements and levels of refinement of, from top to bottom: first order ($N_d = 32$), second order ($N_d = 128$), and third order ($N_d = 512$). Left: sphere discretization. Middle: density on the plane $z = 0.15$. Right: density, view from downwards.

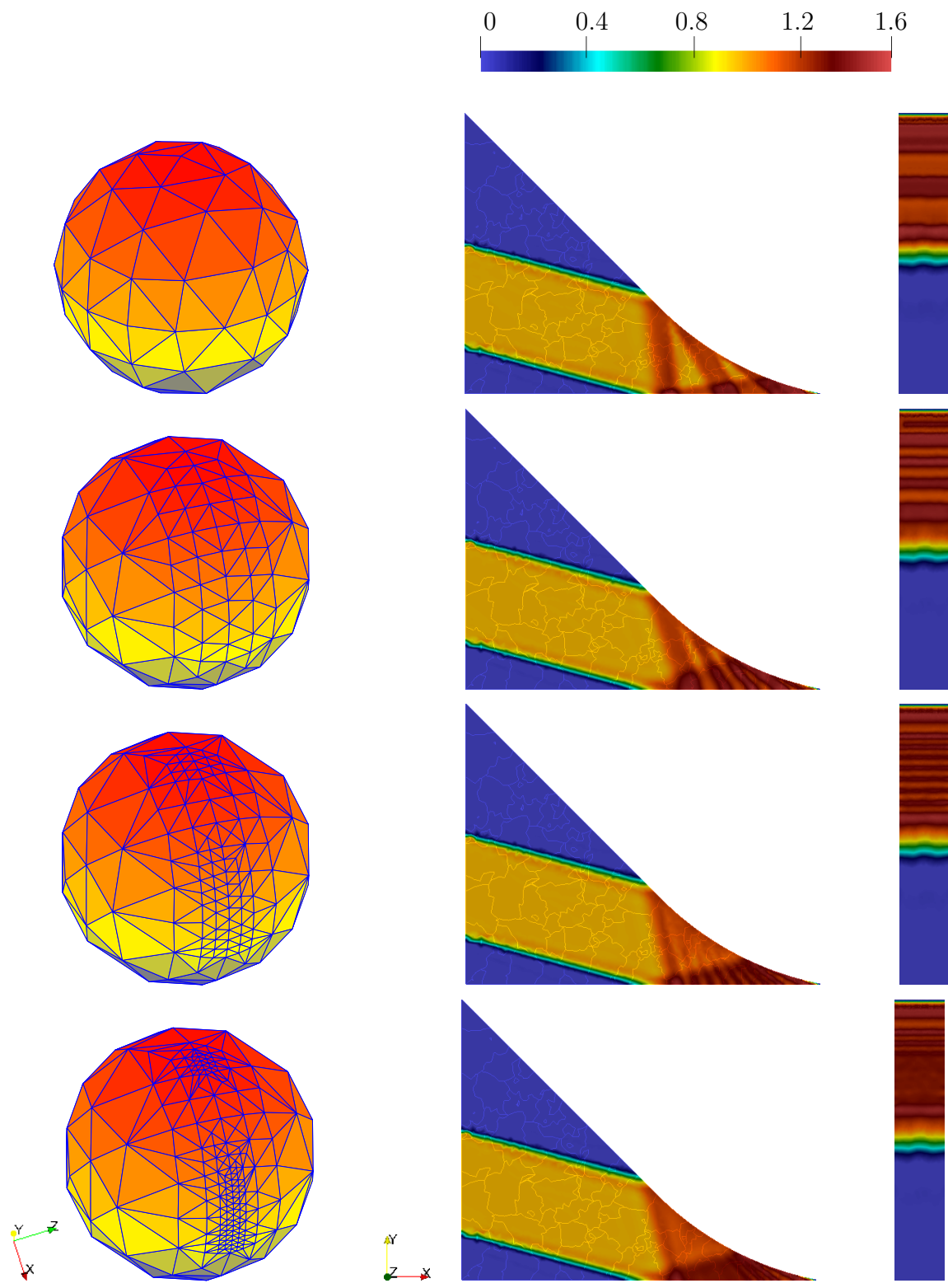


Figure 9: Ad hoc sphere discretizations based on the octahedron, with $\mathbb{P}_{0,v}$ angular finite elements. From top to bottom: $N_d = 66$, $N_d = 101$, $N_d = 137$, and $N_d = 201$. Left: sphere discretization. Middle: density on the plane $z = 0.15$. Right: density, view from downwards.

Contrarily, the ad hoc angular discretization could give smooth maps of radiative densities, in accordance with the involved physics, even with relatively small numbers of directions.

Finally, note that the algorithm is drafted in such a way that it could be easily implemented using pre-existing open-source mathematical libraries, and plugged-in to any existing RTE solver.

7. References

- [1] Y. Favennec, M. Badri, T. Mathew, B. Rousseau, A parallel implicit mixed–fem solution for complex domain radiative transfer problems using immersed meshes, in: Eurotherm Seminar 110 Computational Thermal Radiation in Participating Media - VI April 11-13, 2018, Cascais, Portugal, 2018.
- [2] W. Fiveland, Discrete-ordinates solutions of the radiative transport equation for rectangular enclosures, *Journal of Heat Transfer* 106 (4) (1984) 699–706.
- [3] D. Le Hardy, Y. Favennec, B. Rousseau, F. Hecht, Specular reflection treatment for the 3d radiative transfer equation solved with the discrete ordinates method, *Journal of Computational Physics* 334 (2017) 541–572.
- [4] G. Raithby, E. Chui, A finite-volume method for predicting a radiant heat transfer in enclosures with participating media, *Journal of Heat Transfer* 112 (2) (1990) 415–423.
- [5] R. O. Castro, J. P. Trelles, Spatial and angular finite element method for radiative transfer in participating media, *Journal of Quantitative Spectroscopy and Radiative Transfer* 157 (2015) 81–105.
- [6] P. J. Coelho, A hybrid finite volume/finite element discretization method for the solution of the radiative heat transfer equation, *Journal of Quantitative Spectroscopy and Radiative Transfer* 93 (1) (2005) 89–101.
- [7] S. Richling, E. Meinköhn, N. Kryzhevoi, G. Kanschat, Radiative transfer with finite elements-i. basic method and tests, *Astronomy & Astrophysics* 380 (02) (2001) 776–788.
- [8] D. Le Hardy, M. A. Badri, B. Rousseau, S. Chupin, D. Rochais, Y. Favennec, 3d numerical modelling of the propagation of radiative intensity through a x-ray tomographed ligament, *Journal of Quantitative Spectroscopy and Radiative Transfer* 194 (2017) 86–97.
- [9] M. Badri, P. Jolivet, B. Rousseau, S. Le Corre, H. Dignonnet, Y. Favennec, Vectorial finite elements for solving the radiative transfer equation, *Journal of Quantitative Spectroscopy and Radiative Transfer* 212 (2018) 59–74.
- [10] M. Badri, P. Jolivet, B. Rousseau, Y. Favennec, High performance computation of radiative transfer equation using the finite element method, *Journal of Computational Physics* 360 (2018) 74–92.

- [11] S. Richling, E. Meinköhn, N. Kryzhevoi, G. Kanschat, Radiative transfer with finite elements-i. basic method and tests, *Astronomy & Astrophysics* 380 (02) (2001) 776–788.
- [12] E. Meinköhn, A general-purpose finite element method for 3d radiative transfer problems, in: *Numerical Methods in Multidimensional Radiative Transfer*, Springer, 2009, pp. 99–173.
- [13] G. Widmer, R. Hiptmair, C. Schwab, Sparse adaptive finite elements for radiative transfer, *Journal of Computational Physics* 227 (12) (2008) 6071–6105.
- [14] J. C. Stone, Adaptive discrete-ordinates algorithms and strategies, Ph.D. thesis, Texas A&M University (2008).
- [15] H. Gao, H. Zhao, A fast-forward solver of radiative transfer equation, *Transport Theory and Statistical Physics* 38 (3) (2009) 149–192.
- [16] D. Gorpas, D. Yova, K. Politopoulos, A three-dimensional finite elements approach for the coupled radiative transfer equation and diffusion approximation modeling in fluorescence imaging, *Journal of Quantitative Spectroscopy and Radiative Transfer* 111 (4) (2010) 553–568.
- [17] L. Briggs, W. Miller Jr, E. Lewis, Ray-effect mitigation in discrete ordinate-like angular finite element approximations in neutron transport, *Nuclear Science and Engineering* 57 (3) (1975) 205–217.
- [18] R. Becker, R. Koch, H.-J. Bauer, M. Modest, A finite element treatment of the angular dependency of the even-parity equation of radiative transfer, *Journal of Heat Transfer* 132 (2) (2010) 023404.
- [19] H. Amiri, P. Coelho, A comparison of angular discretization schemes of the hybrid finite volume/finite element method for the solution of the radiative transfer equation, in: *21st Brazilian Congress of Mechanical Engineering*, 2011, pp. 24–28.
- [20] C. Thurgood, A. Pollard, H. Becker, The tn quadrature set for the discrete ordinates method, *Journal of heat transfer* 117 (4) (1995) 1068–1070.
- [21] M. A. Goffin, A. G. Buchan, S. Dargaville, C. C. Pain, P. N. Smith, R. P. Smedley-Stevenson, Goal-based angular adaptivity applied to a wavelet-based discretisation of the neutral particle transport equation, *Journal of Computational Physics* 281 (2015) 1032–1062.
- [22] L. Soucasse, S. Dargaville, A. G. Buchan, C. C. Pain, A goal-based angular adaptivity method for thermal radiation modelling in non grey media, *Journal of Quantitative Spectroscopy and Radiative Transfer* 200 (2017) 215–224.

- [23] J. Kópházi, D. Lathouwers, A space-angle dgfem approach for the boltzmann radiation transport equation with local angular refinement, *Journal of Computational Physics* 297 (2015) 637–668.
- [24] C. Y. Lau, Adaptive discrete-ordinates quadratures based on discontinuous finite elements over spherical quadrilaterals, Ph.D. thesis, Texas A&M University (2016).
- [25] C. Lee, The discrete Sn approximation to transport theory, Tech. rep., Los Alamos Scientific Lab., N. Mex. (1961).
- [26] C. Geuzaine, J. F. Remacle, Gmsh: A 3-D finite element mesh generator with built-in pre-and post-processing facilities, *International journal for numerical methods in engineering* 79 (11) (2009) 1309–1331.
- [27] M. F. Modest, Radiative heat transfer, Academic press, 2013.
- [28] P. Comninos, Mathematical and Computer Programming Techniques for Computer Graphics, Springer, 2006.
- [29] F. Hecht, New development in FreeFem++, *Journal of Numerical Mathematics* 20 (3-4) (2012) 251–266.
- [30] W. Bangerth, R. Hartmann, G. Kanschat, deal.II—a general-purpose object-oriented finite element library, *ACM Transactions on Mathematical Software (TOMS)* 33 (4) (2007) 24.
- [31] B. Patzák, OOFEM: an object-oriented simulation tool for advanced modeling of materials and structures, *Acta Polytechnica* 52 (6).
- [32] V. Dolean, P. Jolivet, F. Nataf, An introduction to domain decomposition methods: algorithms, theory, and parallel implementation, SIAM, 2015.
- [33] J. Truelove, Three-dimensional radiation in absorbing-emitting-scattering media using the discrete-ordinates approximation, *Journal of quantitative spectroscopy and radiative transfer* 39 (1) (1988) 27–31.
- [34] F. Alauzet, P. Frey, Estimateur d’erreur géométrique et métriques anisotropes pour l’adaptation de maillage. partie I: aspects théoriques, Tech. rep., INRIA, RR n° 4759 (2003).
- [35] The Mmg PLATFORM (2018 (accessed August 28, 2018)).
URL <https://www.mmgtools.org/>
- [36] C. Dapogny, C. Dobrzynski, P. Frey, Three-dimensional adaptive domain remeshing, implicit domain meshing, and applications to free and moving boundary problems, *Journal of computational physics* 262 (2014) 358–378.

- [37] B. Lucquin, O. Pironneau, Introduction au calcul scientifique, Masson, 1996.
- [38] B. Mohammadi, P.-L. George, F. Hecht, E. Saltel, 3D mesh adaptation by metric control for CFD, *Revue européenne des éléments finis* 9 (4) (2000) 439–449.
- [39] W. Fiveland, Discrete ordinate methods for radiative heat transfer in isotropically and anisotropically scattering media, *Journal of Heat Transfer (Transactions of the ASME (American Society of Mechanical Engineers), Series C);(United States)* 109 (3).